THESIS FOR THE DEGREE OF DOCTOR OF PHILOSOPHY

# Quantum optics and relativistic motion with superconducting circuits

Joel Lindkvist

Applied Quantum Physics Laboratory
Department of Microtechnology and Nanoscience
CHALMERS UNIVERSITY OF TECHNOLOGY
Göteborg, Sweden 2015

Quantum optics and relativistic motion with superconducting circuits
JOEL LINDKVIST

ISBN 978-91-7597-300-5



Doktorsavhandlingar vid Chalmers tekniska högskola
Ny serie nr 3981
ISSN 0346-718X

Applied Quantum Physics Laboratory
Department of Microtechnology and Nanoscience - MC2
Chalmers University of Technology
SE-412 96 Göteborg, Sweden
Telephone +46 (0)31 772 1000
www.chalmers.se

Author email: joell@chalmers.se

ISSN 1652-0769
Technical Report MC2-323

Printed by Chalmers Reproservice
Göteborg, Sweden 2015

Quantum optics and relativistic motion with superconducting circuits

JOEL LINDKVIST

Applied Quantum Physics Laboratory
Department of Microtechnology and Nanoscience
Chalmers University of Technology

**Abstract**

Superconducting microwave circuits provide a versatile platform for studying quantum optics with artificial atoms, mainly motivated by applications in quantum information. In addition, the circuits are promising for simulation of relativistic phenomena. This thesis is based on theoretical work along both these lines.

Firstly, we consider a transmon coupled to an open transmission line. Using circuit quantization techniques and the master equation formalism, we theoretically describe scattering of coherent microwaves states on the transmon. The results agree with various recent experiments. As an example, we see a photon number redistribution leading to antibunching in the reflected field and superbunching in the transmitted field. Inspired by these results, we further investigate the possibility of generating single-photon states on demand in the system. We find that a single two-level system in an open transmission line is not a suitable single-photon source. With an asymmetric setup using two transmission lines, however, single-photon probabilities close to unity can be achieved.

Secondly, we investigate simulation of a relativistically moving cavity containing a quantum field. Previously, in order to demonstrate the dynamical Casimir effect, a SQUID was used to tune a boundary condition in a way that mimics a moving mirror. Building on this idea, we extend the setup and use two SQUIDs to simulate the moving cavity. An experiment is proposed where the cavity is used as a clock and we show that time dilation should be observable for realistic circuit parameters. We also show how the size and the acceleration of the clock leads to a deviation from the ideal clock formula. Moreover, the effect of acceleration on the precision of the clock is analyzed.

**Keywords:** Superconducting circuits, circuit QED, SQUID, transmon, propagating microwaves, quantum optics, quantum field theory, special relativity, relativistic motion, time dilation

# List of publications

This thesis is based on the work contained in the following papers, which are referred to in the text by their Roman numerals:

I. **Generation of Nonclassical Microwave States Using an Artificial Atom in 1D Open Space**
Io-Chun Hoi, Tauno Palomaki, Joel Lindkvist, Göran Johansson, Per Delsing and C. M. Wilson
*Physical Review Letters* **108**, 263601 (2012)

II. **Microwave quantum optics with an artificial atom in one-dimensional open space**
Io-Chun Hoi, C. M. Wilson, Göran Johansson, Joel Lindkvist, Borja Peropadre, Tauno Palomaki and Per Delsing
*New Journal of Physics* **15**, 025011 (2013)

III. **Scattering of coherent states on a single artificial atom**
Borja Peropadre*, Joel Lindkvist*, Io-Chun Hoi, C. M. Wilson, J. J. Garcia-Ripoll, Per Delsing and Göran Johansson
*New Journal of Physics* **15**, 035009 (2013)
(*Joint first authorship)

IV. **Scattering of coherent pulses on a two-level system– single-photon generation**
Joel Lindkvist and Göran Johansson
*New Journal of Physics* **16**, 055018 (2014)

V. **Twin paradox with macroscopic clocks in superconducting circuits**
Joel Lindkvist, Carlos Sabín, Ivette Fuentes, Andrzej Dragan, Ida-Maria Svensson, Per Delsing and Göran Johansson
*Physical Review A* **90**, 0521138 (2014)

VI. **Motion and gravity effects in the precision of quantum clocks**
Joel Lindkvist, Carlos Sabín, Ivette Fuentes and Göran Johansson
*Scientific Reports* **5**, 10070 (2015)

# Acknowledgements

First and foremost, I would like to thank my supervisor Göran Johansson for guiding me through this work during the past years. I knew nothing about superconducting circuits when I started, but now I allow myself to believe that I at least know something.

The Applied Quantum Physics Laboratory has been a great place spend these years in; a fact that is largely due to all the past and present members of the group. I have really enjoyed our discussions and activities, both work-related and otherwise. The same goes for my collaborators and friends in the Quantum Device Physics Laboratory. Thanks a lot!

I would also like to thank Ivette Fuentes, Carlos Sabín and the rest of the Nottingham group for hosting me during my visits.

Thanks to Göran, Tomas and Oscar for proofreading the thesis and to Maciej for helping out with many practical issues.

Finally, many thanks go to my family, my friends and to Emma.

Göteborg, November 2015
Joel Lindkvist

# Contents

# List of figures

# Nomenclature

**Abbreviations**

| | |
|---|---|
| BCS | Bardeen-Cooper-Schrieffer |
| CPB | Cooper pair box |
| CPW | Coplanar waveguide |
| CQED | Cavity quantum electrodynamics |
| cQED | Circuit quantum electrodynamics |
| DCE | Dynamical Casimir effect |
| EM | Electromagnetic |
| GL | Ginzburg-Landau |
| h.c. | Hermitian conjugate |
| QED | Quantum electrodynamics |
| QFI | Quantum Fisher information |
| QFT | Quantum field theory |
| RQI | Relativistic quantum information |
| RWA | Rotating wave approximation |
| SQUID | Superconducting quantum interference device |
| SR | Special relativity |

# Chapter 1

# Introduction

In quantum optics, light and its interaction with matter is studied at a level where quantum effects are important. Although quantum descriptions of light and atoms date back to the early days of quantum mechanics, it took many years for experiments to reach the point where single photons and atoms can be manipulated and measured. In 2012, Serge Haroche and David Wineland were awarded the Nobel Prize in Physics for their contributions to this development [1, 2]. An important challenge in experimental quantum optics is to reach the *strong coupling regime*, where the atom-photon coupling is much larger than the coupling to the external world. In this case, controlled operations can be performed on the system before information is lost to the environment, which is crucial in many applications. One approach is to confine the light in a cavity, thus enhancing the coupling between atoms and light at the single-photon level. This field of research is known as *cavity quantum electrodynamics* (cavity QED or CQED) [3].

An alternative to performing quantum optics experiments with natural atoms is to use analogue systems based on *artificial atoms* [4]. These are many-particle systems designed to have simple energy level structures, similar to those of single atoms. Setups with artificial atoms can offer several advantages compared to natural atoms; improved control, increased tunability and the possibility of reaching parameter regimes not found in nature. One very promising platform for quantum optics with artificial atoms, and the one that we focus on in this thesis, is *circuit quantum electrodynamics* (circuit QED or cQED) [5–7], which is based on superconducting electrical circuits. The development of circuit QED is outlined

in section 1.1 and in Chapter 2 we give a more thorough introduction to superconducting circuits.

Apart from its relevance for experimentally investigating fundamental aspects of quantum mechanics, development in CQED and in particular cQED has largely been driven by possible applications in quantum information processing. The idea of a computer with an operational principle based on quantum mechanics was first introduced in 1982 by Richard Feynman [8]. A quantum computer is based on quantum bits, or *qubits*, which are quantum mechanical two-level systems. While a classical bit can only take the values 0 and 1, a qubit can exist in a *superposition* of its two eigenstates $|0\rangle$ and $|1\rangle$,

$$|\psi\rangle = a\,|0\rangle + b\,|1\rangle\,, \tag{1.1}$$

where $a$ and $b$ are complex numbers. This can be exploited for *parallelization*, allowing certain computational tasks to be performed much faster on a quantum computer than on a classical one [9]. Developing algorithms [10, 11] for quantum computers is an active field of research, with the most well-known example to date being *Shor's algorithm* for prime factorization [12].

In the past decades, a large effort has gone into the problem of implementing qubits in physical systems. For quantum computing to work, it must be possible to initialize the qubit states, perform one- and two-qubit gate operations and read out the qubit states [13]. Another challenge is to overcome the problem of *decoherence*. Due to interaction with the environment, the superposition state of a qubit is lost after a certain time. Designing qubits with longer coherence times is an active field of research. Apart from CQED and cQED, candidates for quantum computing include trapped ions [14, 15], semiconductor quantum dots [16, 17], NV centers in diamond [18] and atoms in optical lattices [19].

The quest for a quantum computer is only one part of the vast field of quantum information science. Closely related is the idea of *quantum simulations* [20] where, instead of being able to perform different computational tasks, one controllable quantum system simply simulates another quantum system. In addition, there is the field of *quantum communication* [21, 22], aiming to realize quantum-based communication networks. Communication channels able to transmit quantum states can be used for *quantum cryptography* [23, 24].

In the last decade, the emerging field of *relativistic quantum information* (RQI) [25, 26] has gained a considerable amount of attention. In RQI, the effects of special and general relativity [27, 28] on quantum information tasks are investigated. Not only is this interesting from a fundamental standpoint, but also from a more pragmatic point of view. Quantum communication protocols have recently been carried out over long distances on Earth [29] and there are plans to realize similar experiments between satellites [30, 31]. On these macroscopic scales, possible effects of relativity must be taken seriously.

Closely related to RQI is *relativistic quantum metrology* [32]. Quantum metrology aims to exploit quantum physics for high-precision measurements. One example is timekeeping, where quantum mechanics can be used to build more precise clocks [33]. Effects of special and general relativity have since long been measured with atomic clocks [34, 35], and gravitational time dilation is corrected for in the GPS system [36]. These clocks, however, are described by non-relativistic quantum mechanics. Both quantum and relativistic effects can be taken into account within the framework of *quantum field theory* (QFT) [37, 38]. In Papers V and VI, we consider a fundamental clock model based on QFT and investigate how its rate and precision is affected by non-uniform relativistic motion.

Superconducting circuits cannot only be used for circuit QED experiments, but also for simulation of relativistic motion [39, 40]. This is the main topic of Paper V, where we propose an experiment to simulate a moving clock. A longer introduction to this type of simulations is given in section 1.2.

## 1.1 Circuit QED

In circuit QED, quantum optical analogue systems are implemented in superconducting circuits. These circuits are on-chip devices where the circuitry is made of a superconducting material placed on top of a dielectric substrate. The fact that the entire system is an integrated circuit allows for great stability and controllability. Unlike in natural systems, there is no need to trap the atoms and keep them stable. The fabrication of the chips uses lithographic techniques that are well known from conventional circuit fabrication.

The artificial atoms in cQED are small circuits designed to have an atom-like level structure. Despite being macroscopic, these circuits can

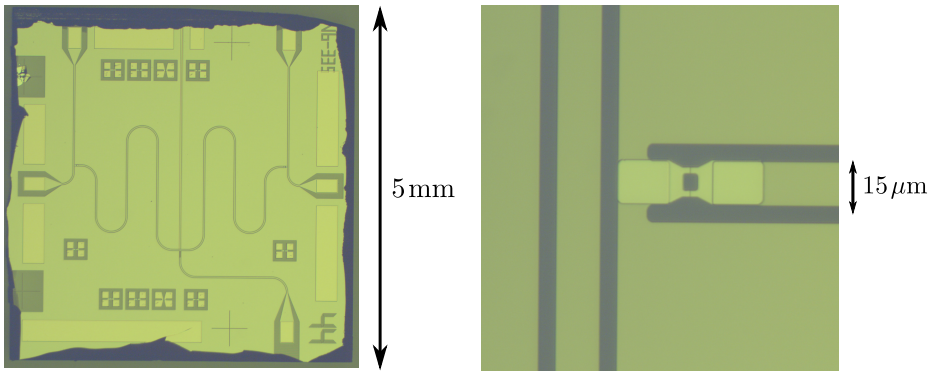


Figure 1.1: Optical micrograph of a chip containing the circuit used to implement the results of Paper V. The brighter areas are superconducting, while the darker areas are dielectric. The left figure shows the entire chip, where the meandered structure is a coplanar waveguide terminated at both ends to form a cavity. The right figure shows two Josephson junctions forming a SQUID at the end of the coplanar waveguide. A separate waveguide is used to generate a magnetic flux through the SQUID. Pictures by Ida-Maria Svensson.

for low enough temperatures exhibit quantum behavior. There are many ways to design superconducting artificial atoms, each with their advantages and disadvantages. What they all have in common is that they are based on the *Josephson junction* [41], which is a nonlinear inductive circuit element. The superconducting artificial atoms typically have transition frequencies in the microwave (GHz) range. This means that standard equipment from microwave technology can be used for signal generation and amplification. The atoms are connected by transmission lines, in the form of *coplanar waveguides* [42], for the electromagnetic field. These can be seen as squashed coaxial cables, with a center conductor between two ground planes. Figure 1.1 shows a chip with the circuit studied in Paper V. The (meandered) coplanar waveguide can clearly be seen, and the zoom-in shows two Josephson junctions forming a so-called SQUID (see section 2.5). In order to exhibit quantum behavior, these circuits must be operated in cryostats at temperatures around 50 mK.

Since superconducting artificial atoms in most applications are used as qubits, with only two levels addressed, we will often refer to them as superconducting qubits. One drawback of these qubits is that, being macroscopic, they couple strongly to the environment, leading to decoherence.

This means that they generally have shorter coherence times than natural atoms. The first experimental demonstration of coherent control of a superconducting qubit, the so-called *charge qubit*, was performed in 1999 [43]. Since then, much effort has gone into developing qubits with longer coherence times, both theoretically and experimentally. Other than the charge qubit, early superconducting qubit designs include the *flux qubit* [44, 45] and the *phase qubit* [46]. For a review of these three types of qubits, see [47].

A later development of the charge qubit, known as the *transmon* [48], shows a significantly reduced sensitivity to charge noise. This increases the coherence time, making the transmon a popular choice among the superconducting qubits. Part of the work in this thesis concerns systems with transmons, experimentally (Papers I & II) and theoretically (Paper III). Even longer coherence times are achieved by coupling transmons to 3D cavities [49]. The last decade has seen coherence times of superconducting qubits increase with several orders of magnitude, and they start to reach the regime where quantum computing is possible. To actually build a working quantum computer with superconducting circuits, however, remains an enormous technological challenge [50].

Since the coplanar waveguides are effectively one-dimensional transmission lines, circuit QED systems show a good confinement of the electric field. Together with the fact that the effective dipole moments of the artificial atoms can be large by design, this makes it easier to achieve strong coupling between single photons and atoms than in natural cavity QED setups [6]. Moreover, by the use of SQUIDs, the transition frequencies and coupling strengths cannot only be chosen by design, but also tuned *in situ*.

Most experiments in circuit QED have made use of a coplanar waveguide terminated in both ends to form a cavity, where the atom interacts with discrete field modes. In the quantum computing applications, the artificial atoms play the roles of qubits while the photons are used for qubit manipulation and readout. Recently, however, there has been a growing interest in artificial atoms interacting with propagating photons in open transmission lines [51–56]. These systems can be used to realize quantum communication networks [57] and potentially for all-optical quantum computing [58]. Here, the roles of the photons and the atoms are reversed; the qubit is represented by the photon, whereas the atoms are used to manipulate the photon states. The system studied in Papers I-IV is a transmon

interacting with propagating photons in an open transmission line.

In order to realize quantum information protocols with propagating microwave photons, it must be possible to routinely generate and detect single photons. Due to the lower energy of the photons, photodetectors are more difficult to realize for microwaves than in the optical regime. Theoretical proposals of single-photon detectors based on qubits [59–61] and transmons [62] have been made, but not yet realized experimentally. Generation of single-photon states have been realized in different experiments [63–66], but these all make use of a cavity that limits the bandwidth of operation. Paper I is an experimental study of a transmon coupled to an open transmission line, where it is shown that nonclassical photon states can be generated in the system. Inspired by this, we propose a non-cavity based single-photon source in Paper IV.

A growing trend in quantum information processing is that of *hybrid systems* [67]. By combining several physical systems, it is possible to exploit the advantages and avoid the disadvantages of each system. In most cases, superconducting circuits are included due to their controllability and strong coupling to external fields. Optical photons in fibers, on the other hand, are suitable for long-distance communication. For storing of information, in a *quantum memory* [68], natural atoms or spins are more suitable than superconducting circuits due to their longer coherence times. Finding interfaces to transfer quantum information between the systems is an active area of research. Another example is *quantum electromechanics* [69], where the circuits are coupled to mechanical systems. Closely related is *quantum optomechanics* [70], where photons interact with mechanical resonators. Controlling mechanical systems at the quantum level is of fundamental interest, since it may be used to study decoherence of macroscopic objects, a fundamental problem in quantum mechanics. In particular, the systems can possibly be used to test models of *gravitationally induced decoherence* [71–73]. Such experiments would increase our understanding of the relation between quantum mechanics and general relativity, which remains one of the biggest open questions in modern physics.

## 1.2 Relativistic motion in superconducting circuits

As mentioned in section 1.1, SQUIDs can be used to tune transition frequencies and coupling strengths in circuit QED. This tunability is also

useful in a different context, when the SQUID is operated as a boundary condition for the quantum field in a coplanar waveguide. By modulating the magnetic flux in the SQUID, the boundary condition can be made to mimic that of a mirror moving at relativistic speeds. In 2011, this trick was used to experimentally demonstrate the dynamical Casimir effect (DCE) for the first time [39]. The DCE is a prediction of quantum field theory, stating that photons are created from the vacuum when there are time-dependent boundary conditions [74]. Due to the difficulty in moving massive mirrors fast enough, though, it had never been observed before.

The setup used to demonstrate the DCE can be extended to simulate a moving one-dimensional cavity, by use of two SQUIDs. Moving cavities containing quantum fields have been studied in the context of RQI, to investigate relativistic effects on quantum entanglement [75–79] and teleportation protocols [40]. In Papers V and VI, we let a cavity of this type play the role of a fundamental clock and propose an experiment to simulate time dilation effects in superconducting circuits. Possibly, more predictions from RQI can be tested using these simulations in the future.

Modulation of boundary conditions is not the only way to simulate relativistic physics with superconducting circuits. Relativistic motion of qubits [80] has been suggested to study effects similar to the Unruh effect [81, 82]. Another example, involving general relativity, is the proposal to simulate Hawking radiation [83, 84] by using a SQUID array to create an event horizon [85].

## 1.3 Outline of the thesis

In this section, we give an overview of the content in the following chapters. Since this is a *compilation thesis*, the scientific results are included mainly in the appended papers. The preceding chapters serve to give the reader a background in the different subject areas, necessary to understand the papers.

Chapter 2 treats superconducting circuits, which in some way relates to all the appended papers. Starting with a brief introduction to superconductivity, we then outline how to quantize electrical circuits. Next, the fundamental circuit elements (capacitance, inductance and Josephson junction) are introduced and in the subsequent sections we describe the important components of the systems studied in the papers; the SQUID, the transmission line and the transmon.

Chapter 3 starts with an introduction to special relativity. We then go on to discuss time dilation and accelerated clocks. Finally, we discuss rigid body motion in relativity. All these concepts relate to the clock model used in Papers V and VI, which is a rigid cavity undergoing accelerated motion.

Chapter 4 treats the one-dimensional massless Klein-Gordon field, which is the effective description of the electromagnetic field used in all the appended papers. We start by describing the quantization of the field in open space, with a continuous spectrum, and in a cavity, with a discrete spectrum. Next, the interaction of the field with atoms, used in Papers I-IV is discussed. In the subsequent sections, different types of states are described. First, we focus on discrete mode states, among them the Gaussian states that are important in our description of the moving cavity in Papers V and VI. The following section is devoted to continuous mode states, relevant for Papers I-IV, and how to characterize them using coherence functions. We end with a treatment of the Klein-Gordon field in noninertial reference frames and describe how to use Bogoliubov transformations to transform between different frames. These techniques are used in Papers V and VI.

In Chapter 5, we treat open quantum systems. To describe the evolution of a system under the influence of its surroundings, like the electromagnetic field, we introduce the master equation. To accompany the master equation, we also derive input-output equations for the signal being scattered from the system. These formalisms are used in the treatment of atom-field interactions in Papers I-IV.

Finally, Chapter 6 contains an overview of each of the appended papers and in Chapter 7 we summarize our work and give a brief outlook.

# Chapter 2

# Superconducting circuits

As we saw in Chapter 1, superconducting circuits can be used for quantum optics experiments and quantum information tasks, as well as simulation of relativistic effects. Although the devices contain a macroscopic number of atoms, their low-energy behaviour can effectively be described by a few collective degrees of freedom. The systems described by these degrees of freedom typically have characteristic frequencies in the GHz range and when operated at low enough temperatures, that is 10-50 mK, they can exhibit quantum behaviour. In this sense, macroscopic quantum phenomena can be observed in superconducting circuits.

In section 2.1 we give a brief introduction to superconductivity and introduce the lumped-element description of circuits. For a more extensive introduction to superconductivity, see [86]. In the remaining sections of this chapter, the quantization procedure is described, mainly following [87], and all the relevant circuit elements are introduced.

## 2.1 Superconductivity

When cooled below a critical temperature, certain metals become *superconducting* [86]. In this state of matter, two basic phenomena emerge. The first is zero electrical resistance, making it possible for a current to flow without dissipation, and the second is the expulsion of magnetic fields from the interior of the material, known as the *Meissner effect*.

A microscopic theory of so-called *conventional* superconductors was developed in 1957 by Bardeen, Cooper and Schrieffer (BCS) [88]. In BCS theory, the electrons in the superconductor are paired into *Cooper pairs*

[89] due to a phonon-mediated attractive interaction. The Cooper pairs form a condensate and there is a certain energy cost of breaking a pair to form a single-particle excitation. This results in an *energy gap* $\Delta$ between the ground state and the lowest excited state of the superconductor. For energies well below the gap, the degrees of freedom are thus significantly reduced.

Ginzburg-Landau (GL) theory was originally introduced as a phenomenological theory describing the macroscopic degrees of freedom of the superconducting state, but was later shown to be a consquence of BCS theory. In GL theory, the central object is the complex order parameter $\psi(r)$, defined so that $|\psi(r)|^2$ represents the local density of superconducting electrons. Moreover, the phase of $\psi(r)$ is important when describing Josephson junctions (see section 2.4).

Now, consider a superconducting circuit with physical dimensions much smaller than the shortest wavelength of the currents and voltages of interest. In this case, we can neglect retardation effects and assume instantaneous propagation of signals in the circuit. The different electromagnetic phenomena, like generation of electric and magnetic fields, can then be represented by *lumped elements*. In this way, we go from a description with a continuous charge density distribution $|\psi(r)|^2$ to a simpler description where the electron fluid moves rigidly and charges can only be accumulated on a discrete number of nodes. This further reduces the degrees of freedom of the circuit. The immense reduction of degrees of freedom, made possible by both the superconductivity and the lumped-element approximation, allows us to design macroscopic circuits behaving as single harmonic or anharmonic oscillators. It is this fact that enables us to construct artificial atoms, as we will see in section 2.7.

## 2.2 Circuit quantization

A systematic way to quantize an electrical circuit in the lumped-element approximation was described in [87, 90]. Here, we will outline the main steps of this approach. The first step is to choose a set of generalized coordinates and write down the Lagrangian $\mathcal{L} = T - U$, where $T$ is the kinetic energy and $U$ the potential energy. The degrees of freedom in a classical circuit are usually described in terms of the voltages $V(t)$ and currents $I(t)$ associated with the circuit branches. These are constrained by Kirchoff's laws. An independent set of variables can be obtained by

identifying the nodes of the circuit and assigning a coordinate to each node. One possibility is to use the node charge $Q(t)$, related to the current $I(t)$ through the node by

$$Q(t) = \int_{-\infty}^{t} I(t')dt', \tag{2.1}$$

as the generalized coordinate. In the following, however, we will mostly describe circuits containing nonlinear elements (i. e. Josephson junctions) for which it proves more convenient to use the flux $\Phi(t)$ of the node as coordinate. The flux is related to the voltage $V(t)$ at the node, relative to an arbitrary ground node, by

$$\Phi(t) = \int_{-\infty}^{t} V(t')dt'. \tag{2.2}$$

Indexing the nodes by $i$, the fluxes $\Phi_i$ constitute a set of generalized position coordinates that can be used to describe the Lagrangian dynamics of the circuit. From the Lagrangian $\mathcal{L}$, the Hamiltonian $\mathcal{H}$ is obtained through the Legendre transformation

$$\mathcal{H} = \sum_i Q_i \dot{\Phi}_i - \mathcal{L}, \tag{2.3}$$

with $Q_i = \frac{\partial L}{\partial \dot{\Phi}_i}$ being the generalized momenta. Using the node flux as generalized coordinate, $Q_i$ can be identified as the node charge (2.1). The flux and the charge of each node are thus canonically conjugate quantities.

To step to a quantum mechanical description, $\Phi_i$ and $Q_i$ are promoted to operators obeying the canonical commutation relations [91]

$$[\Phi_i,Q_j] = i\hbar\delta_{ij}, \tag{2.4}$$

with $\hbar = h/2\pi$, where $h$ is Planck's constant.

## 2.3 Capacitance and inductance

Capacitances and inductances are two basic circuit elements with different voltage-current relations. In this section, we describe these elements and write down standard expressions for their Lagrangians in terms of node fluxes. We let $\Phi$ denote the flux drop over the element, i. e. the difference in flux between the two nodes.


Figure 2.1: The circuit symbols for capacitance $C$ and inductance $L$.

A capacitance $C$ is assigned to a device where energy is stored in the electric field between two charged conductors separated by an insulator. The voltage drop over the capacitance is proportional to the stored charge $Q$ according to $V = CQ$. In terms of $\Phi$, the stored energy can be expressed as

$$E_C = \frac{1}{2} C \dot{\Phi}^2. \tag{2.5}$$

Thus, each capacitance corresponds to a kinetic term in the Lagrangian.

An inductance $L$ is assigned to a device where energy is stored in the magnetic field generated by moving charges. The voltage drop over the inductance is proportional to the time-derivative of the current via the relation $V = L\dot{I}$. In terms of $\Phi$, the stored energy can be expressed as

$$E_L = \frac{1}{2L} \Phi^2. \tag{2.6}$$

Thus, each inductance corresponds to a potential term in the circuit Lagrangian. The standard circuit symbols for capacitance and inductance are shown in figure 2.1.

## 2.4 Josephson junctions

A Josephson junction consists of two superconductors coupled by a weak link, which can be a thin layer of insulating material or a normal metal. In a groundbreaking paper from 1962 [41], Josephson showed that Cooper pairs can tunnel through the link, giving rise to several interesting phenomena. In contrary to conventional circuit elements, current can flow even when there is no voltage drop over the junction. This is the so-called DC Josephson effect. Letting $\phi(t)$ denote the difference in the phase of the Ginzburg-Landau order parameter on the two sides of the junction, the current is given by

$$I(t) = I_c \sin \phi(t), \tag{2.7}$$

where $I_c$ is a parameter of the junction known as the critical current. This is the maximal supercurrent through the junction, i. e. current that can flow without resistance. When $I_c$ is exceeded, the current partly consists of quasiparticle tunneling and the junction becomes resistive [92]. In a voltage-biased junction, the phase difference evolves in time according to

$$\dot{\phi}(t) = \frac{2\pi}{\Phi_0} V(t), \tag{2.8}$$

where $\Phi_0 = h/2e$ is the magnetic flux quantum. For a constant voltage-bias $V$, the phase difference evolves as $\phi(t) = 2\pi V t/\Phi_0$ and consequently, the current through the junction varies harmonically in time. This is called the AC Josephson effect. Sometimes (2.7) and (2.8) are referred to as the DC and AC Josephson relations, respectively.

Comparing (2.2) and (2.8), we note that the phase and flux drops are related by $\phi = 2\pi\Phi/\Phi_0$. We can thus easily incorporate Jospehson junctions into the Lagrangian description of circuits outlined in section 2.2. Using (2.7) and (2.8), the voltage drop can be written as

$$V = \frac{\Phi_0}{2\pi}\dot{\phi} = \frac{\Phi_0}{2\pi}\frac{1}{I_c \cos\phi}\dot{I} \tag{2.9}$$

and we can therefore think of the Josephson junction as an inductor, with *nonlinear* inductance

$$L_J = \frac{\Phi_0}{2\pi}\frac{1}{I_c \cos\phi}. \tag{2.10}$$

The nonlinear properties of the Josephson junction are crucial in the design of artificial atoms, allowing quantum optics experiments and quantum information tasks to be performed in superconducting circuits.

To obtain an expression for the energy $U_J$ stored in a Josephson junction, we integrate the power $P = IV$ over time. Again using (2.7) and (2.8), this results in

$$\begin{aligned} U_J &= \int_{-\infty}^{t} I(t')V(t')dt' = \frac{\Phi_0 I_c}{2\pi}\int_{-\infty}^{t}\frac{d\phi}{dt'}\sin\phi(t')dt' \\ &= \frac{\Phi_0 I_c}{2\pi}\int_0^{\phi}\sin\phi' d\phi' = E_J(1-\cos\phi), \end{aligned} \tag{2.11}$$

where we have defined the Josephson energy $E_J = \Phi_0 I_c/2\pi$. Thus, using the node fluxes as generalized coordinates, a Josephson junction corresponds to a potential term in the Lagrangian. This is, in fact, the great

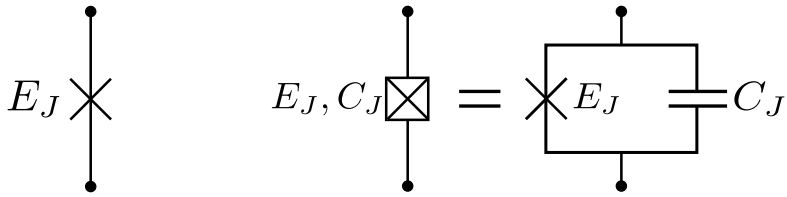


Figure 2.2: Left: The circuit symbol for an ideal Josephson junction with Josephson energy $E_J$. Right: The circuit symbol for a junction with Josephson energy $E_J$ and capacitance $C_J$.

advantage of using the node fluxes as generalized coordinates instead of the node charges.

Above, we have described ideal Josephson junctions. A physical junction, however, also has capacitive properties and is modelled by a nonlinear inductance in parallel with a capacitance $C_J$. The Lagrangian thus becomes

$$\mathcal{L}_J = \frac{1}{2} C_J \dot{\Phi}^2 - E_J \left(1 - \cos\left(2\pi\Phi/\Phi_0\right)\right). \tag{2.12}$$

As shown in figure 2.2, the circuit symbol for an ideal Josephon junction is a cross, while the "x-box" symbolizes a tunnel junction in parallel with a capacitance.

Consider now the case when the phase drop over the Josephson junction is small, so that the current $I$ is small compared to $I_c$. In this case, we can linearize the nonlinear Josephson inductance by expanding the cosine in (2.12) to second order, resulting in the Lagrangian

$$\mathcal{L} = \frac{1}{2} C_J \dot{\Phi}^2 - \frac{1}{2} \left(\frac{2\pi}{\Phi_0}\right)^2 E_J \Phi^2. \tag{2.13}$$

This corresponds to a simple harmonic LC-oscillator with eigenfrequency

$$\omega_p = 2\pi \sqrt{\frac{E_J}{\Phi_0^2 C_J}}, \tag{2.14}$$

which is known as the *plasma frequency* of the junction.

## 2.5 SQUIDs

A superconducting quantum interference device (SQUID) is a superconducting loop interrupted by one or several Josephson junctions. SQUIDs

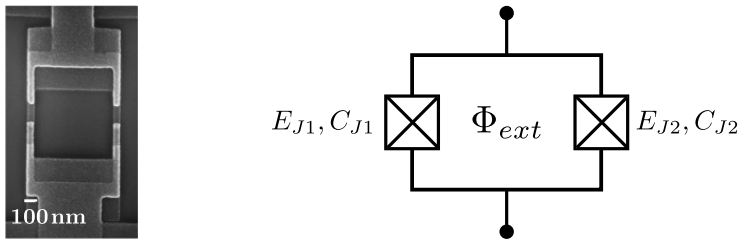


Figure 2.3: Left: Scanning-electron micrograph of the DC SQUID used for the experiments in Paper I. Picture taken from Paper I. Right: Circuit diagram of a DC SQUID with negligible self-inductance.

are primarily used as extremely sensetive magnetometers in a variety of different contexts. For our purposes, as we will see below, their importance lies in the fact that they can be operated as *tunable* Josephson junctions.

The interesting properties of a SQUID are based on the phenomenon of *fluxoid quantization* [86]. Since the Ginzburg-Landau order parameter must be a single-valued function, the phase $\phi$ of the condensate can only change by multiples of $2\pi$ when completing a loop. This implies that a quantity known as the *fluxoid* is quantized in integer multiples of the magnetic flux quantum $\Phi_0$. Written out explicitly, the fluxoid for a SQUID with $N$ Josephson junctions is

$$\Phi' = \Phi_{\text{ext}} + \Phi_{\text{ind}} + \frac{\Phi_0}{2\pi} \sum_{i=1}^{N} \phi_i, \tag{2.15}$$

where $\Phi_{\text{ext}}$ is the external magnetic flux through the loop, $\Phi_{\text{ind}}$ is the flux induced by a circulating current and $\phi_i$ are the phase differences across the Josephson junctions.

In the following, we will limit our analysis to two-junction loops, also known as DC SQUIDs. Figure 2.3 shows a picture of a DC SQUID, as well as the circuit diagram. In the case of a symmetric SQUID, where both Josephson junctions have the same capacitance $C_J$ and Josephson energy $E_J$, the Lagrangian is

$$\mathcal{L} = \frac{1}{2} C_J \left( \dot{\Phi}_1^2 + \dot{\Phi}_2^2 \right) + E_J \left[ \cos\left(2\pi\Phi_1/\Phi_0\right) + \cos\left(2\pi\Phi_2/\Phi_0\right) \right], \tag{2.16}$$

where the constant terms in the potential have been dropped. Now, due to the fluxoid quantization condition, $\Phi_1$ and $\Phi_2$ are not independent variables. If the loop is small enough, we can neglect the induced magnetic

flux $\Phi_{\text{ind}}$ in (2.15), resulting in the condition

$$\Phi_1 - \Phi_2 + \Phi_{\text{ext}} = n\Phi_0. \tag{2.17}$$

Here, the integer $n$ determining the number of flux quanta in the loop depends on the external flux $\Phi_{\text{ext}}$ according to

$$(n - \frac{1}{2})\Phi_0 < \Phi_{\text{ext}} < (n + \frac{1}{2})\Phi_0. \tag{2.18}$$

To implement the fluxoid quantization condition, we introduce the new variable $\Phi = \frac{1}{2}(\Phi_1 + \Phi_2)$. Together with (2.17), this implies

$$\Phi_1 = \Phi - \frac{1}{2}(\Phi_{\text{ext}} - n\Phi_0), \tag{2.19}$$

$$\Phi_2 = \Phi + \frac{1}{2}(\Phi_{\text{ext}} - n\Phi_0). \tag{2.20}$$

Inserting (2.19) and (2.20) into (2.16) and simplifying, we obtain

$$\mathcal{L} = C_J\dot{\Phi}^2 + 2E_J\left|\cos\left(\frac{\pi}{\Phi_0}\Phi_{\text{ext}}\right)\right|\cos\left(\frac{2\pi}{\Phi_0}\Phi\right). \tag{2.21}$$

Here, we have neglected terms containing only $\Phi_{\text{ext}}$, since they do not affect the dynamics of the system. Now, comparing (2.21) to (2.12), we see that the symmetric DC SQUID behaves as a single Josephson junction, with capacitance $2C_J$ and *tunable* Josephson energy

$$E_J(\Phi_{\text{ext}}) = 2E_J\left|\cos\left(\frac{\pi}{\Phi_0}\Phi_{\text{ext}}\right)\right|, \tag{2.22}$$

which we have plotted in figure 2.4. The effective Josephson energy, or equivalently the critical current, can thus be tuned by modulating the external magnetic flux through the loop. This tunability is important in many applications. In circuit QED, it allows the parameters of the artificial atoms to be tuned *in situ*. Moreover, it can be exploited to generate tunable boundary conditions for quantum fields in waveguides, as we will see in section 2.6.1. In practice, the external magnetic flux is usually generated by sending a current through a separate line on the chip, giving rise to a magnetic field.

In order to intuitively understand the flux-dependence of (2.22), we recall that the critical current $I_c$ of a Josephson junction is the maximal current that can flow through the junction by Cooper pair tunnelling. In a

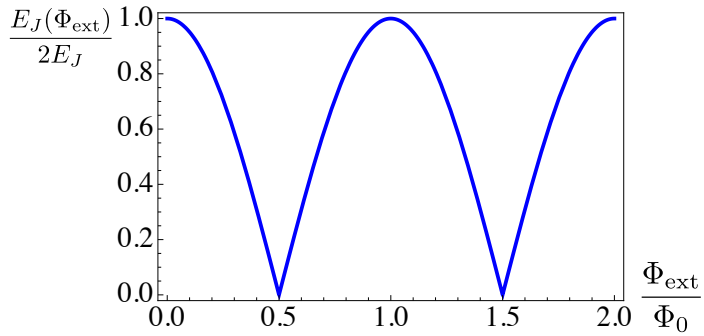


Figure 2.4: Effective Josephson energy $E_J(\Phi_{\text{ext}})$ of a symmetric DC SQUID as a function of the external flux $\Phi_{\text{ext}}$.

symmetric DC SQUID without external flux, a bias current will split into two equal parts, resulting in an effective critical current of $2I_c$. Applying a small flux $\Phi_{\text{ext}}$ will result in a circulating screening current which, through the DC Jospehson relation (2.7), gives rise to phase drops over the junctions to keep the value of the fluxoid (2.17) equal to zero. This current flows in different directions in the two branches of the loop and as a result, the amount of additional current that can flow before exceeding the critical current in one of the Josephson junctions decreases. As $\Phi_{\text{ext}} \to \Phi_0/2$, the screening current approaches $I_c$, so that the effective critical current of the SQUID approaches zero. For $\Phi_{\text{ext}} > \Phi_0/2$ the screening current will reverse direction, to instead satisfy (2.17) with $n = 1$. Increasing $\Phi_{\text{ext}}$ even further will now decrease the screening current until it is zero again at $\Phi_{\text{ext}} = \Phi_0$. This takes us back to the initial situation, albeit with one fluxoid quantum trapped in the loop instead of zero.

## 2.6 Transmission lines

In a transmission line, or waveguide, electromagnetic waves are transferred from one point to another. In on-chip superconducting circuits, the *coplanar waveguide* (CPW) [42] is widely used for this purpose. A CPW consists of a center conductor between two ground planes, as seen in figure 2.5(a).

Since a transmission line is typically longer than the wavelength of the field, it cannot be treated as a single lumped element. By dividing it into small parts, however, it is possible to describe it using the procedure in section 2.2. Figure 2.5(b) shows the circuit diagram of a CPW, with an

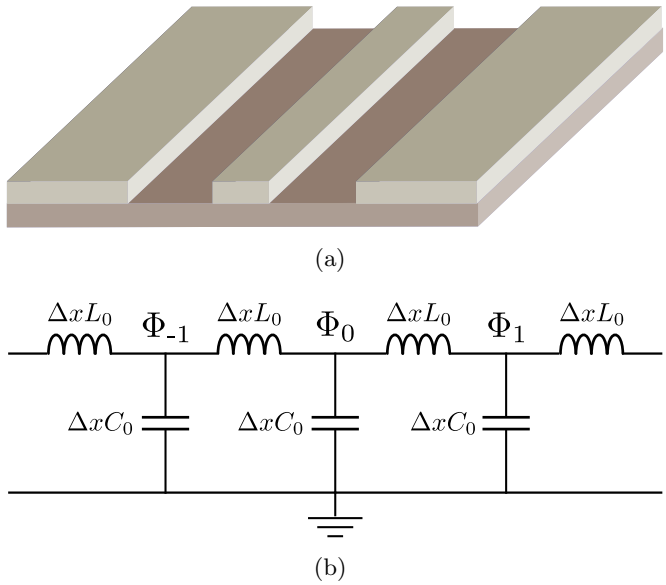


Figure 2.5: (a) Sketch of a coplanar waveguide, consisting of a center conductor between two ground planes. (b) Circuit model of a coplanar waveguide with capacitance $C_0$ and inductance $L_0$ per unit length.

inductance $L_0$ and capacitance $C_0$ per unit length. If $\Delta x$ is taken to be small enough, the field is approximately constant in each interval. This is the requirement for the lumped-element description to be valid. The Lagrangian of the CPW is

$$\mathcal{L}_{CPW} = \sum_n \left( \frac{1}{2} \Delta x C_0 \dot{\Phi}_n^2 - \frac{1}{2\Delta x L_0} \left( \Phi_{n+1} - \Phi_n \right)^2 \right). \tag{2.23}$$

With the conjugate momenta $Q_n = \Delta x C_0 \dot{\Phi}_n$, the Hamiltonian becomes

$$\mathcal{H}_{CPW} = \sum_n \left( \frac{Q_n^2}{2\Delta x C_0} + \frac{\left( \Phi_{n+1} - \Phi_n \right)^2}{2\Delta x L_0} \right). \tag{2.24}$$

Next, we take the continuum limit $\Delta x \to dx$. In this limit, $\Phi_n(t)$ becomes a *flux field* $\Phi(t,x)$ and $Q_n(t)/\Delta x$ a *charge density field* $Q(t,x)$. The continuum Hamiltonian is

$$\mathcal{H} = \frac{1}{2} \int dx \left( \frac{Q^2(t,x)}{C_0} + \frac{\left( \partial_x \Phi(t,x) \right)^2}{L_0} \right). \tag{2.25}$$

Now, $\Phi(t,x)$ and $Q(t,x)$ are our canonical field operators, satisfying the equal-time commutation relation

$$[\Phi(t,x), Q(t,x')] = i\hbar\delta(x - x'). \tag{2.26}$$

Using the Heisenberg equations of motion and (2.26), we obtain $\partial_t\Phi(t,x) = Q(t,x)/C_0$ and $\partial_t Q(t,x) = \partial_x^2\Phi(t,x)/L_0$, implying

$$\left(\partial_t^2 - \frac{1}{L_0C_0}\partial_x^2\right)\Phi(t,x) = 0, \tag{2.27}$$

which is the massless Klein-Gordon equation [37]. Thus, we can conclude that the flux field $\Phi(t,x)$ in the coplanar waveguide behaves as a one-dimensional massless Klein-Gordon field propagating at a velocity

$$c = 1/\sqrt{L_0C_0}. \tag{2.28}$$

For a thorough discussion of the Klein-Gordon field, see Chapter 4. In the quantum description, we will use the term *photon* for an excitation of this field. For typical circuit parameters, the value of $c$ is of the same order of magnitude as the speed of light in vacuum.

### 2.6.1 Boundary conditions

By terminating the CPW in different ways, various boundary conditions for the flux field can be realized. Grounding the waveguide at the endpoint $x = 0$ gives rise to the *Dirichlet* boundary condition $\Phi(t,0) = 0$. This is the same boundary condition that a perfectly conducting mirror imposes on an electromagnetic field. In contrast, leaving the waveguide open ended results in the *Neumann* boundary condition $\partial_x\Phi(t,x)|_{x=0} = 0$. A cavity is formed by terminating both ends of the CPW, allowing cavity QED-like experiments to be performed in circuit QED [5].

Consider now the slightly more complicated case of terminating the CPW via a DC SQUID, as shown in figure 2.6. After linearizing the cosine potential like in (2.13), a circuit analysis of the setup shows that the boundary condition for the field becomes [93]

$$C_J\partial_t^2\Phi(t,0) + \left(\frac{2\pi}{\Phi_0}\right)E_J(\Phi_{\text{ext}})\Phi(t,0) + \frac{1}{L_0}\partial_x\Phi(t,x)\,|_{x=0} = 0, \tag{2.29}$$

where $E_J(\Phi_{\text{ext}})$ and $C_J$ is the effective Josephson energy and capacitance of the SQUID. Now, (2.29) can be rewritten as

$$\frac{1}{\omega_p^2}\partial_t^2\Phi(t,0) + \Phi(t,0) + L_{\text{eff}}(\Phi_{\text{ext}})\partial_x\Phi(t,x)\,|_{x=0} = 0, \tag{2.30}$$

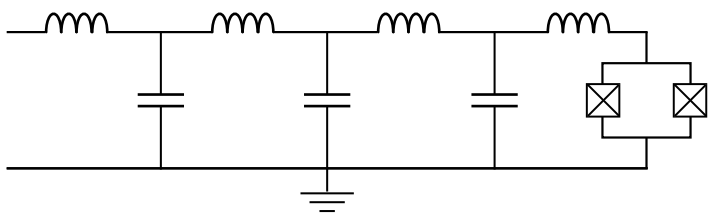

Figure 2.6: Circuit diagram of a coplanar waveguide terminated by a DC SQUID.

where $\omega_p$ is the plasma frequency (2.14) and

$$L_{\text{eff}}(\Phi_{\text{ext}}) = \left(\frac{2\pi}{\Phi_0}\right)^2 \frac{1}{L_0 E_J(\Phi_{\text{ext}})}, \tag{2.31}$$

can be interpreted as an effective length, as we will see shortly. If the plasma frequency is far higher than all the other frequencies involved, the first term in (2.30) can be neglected. We are left with

$$\Phi(t,0) + L_{\text{eff}}(\Phi_{\text{ext}})\partial_x \Phi(t,x) \mid_{x=0} = 0, \tag{2.32}$$

which is known as a *Robin* boundary condition. Now, if $L_{\text{eff}}(\Phi_{\text{ext}})$ is small compared to the wavelength of the field, (2.32) is a good approximation of

$$\Phi\left(t, L_{\text{eff}}(\Phi_{\text{ext}})\right) = 0, \tag{2.33}$$

which is a Dirichlet boundary condition at a *different effective position* than the physical position of the SQUID. By modulating the external flux $\Phi_{\text{ext}}$, this effective position can be dynamically tuned. Thus, for frequencies satisfying $\omega \ll \omega_p$ and $\omega \ll c/L_{\text{eff}}(\Phi_{\text{ext}})$, a boundary condition corresponding to a moving mirror can be generated by means of a SQUID. The mirror can effectively be moved at velocities where relativistic effects become important. In 2011, this was exploited to demonstrate the dynamical Casimir effect [39, 93, 94] and in [40] it was suggested that a moving cavity can be simulated by the use of two SQUIDs. In Paper V, we propose an experiment involving this type of cavity.

## 2.7 Superconducting artificial atoms - the transmon

By using only standard capacitances and inductances, a circuit behaving like a harmonic oscillator, with an equidistant energy spectrum, can be

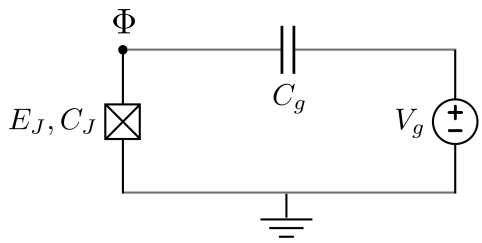


Figure 2.7: Circuit diagram of a Cooper pair box with gate voltage $V_g$. The superconducting island is represented by the node with flux $\Phi$.

designed. An artificial atom suitable for quantum optics experiments and quantum information, however, must have a non-equidistant spectrum. In order to achieve this, some kind of nonlinearity is required, and this is provided by the Josephson junction. As mentioned in Chapter 1, there are several ways to design Josephson junction based artificial atoms. In the following, we will exclusively deal with the *transmon* [48], which is a variant of the *Cooper pair box* (CPB) [95]. A CPB consists of a small superconducting island coupled to a superconducting reservoir via a Josephson junction, allowing Cooper pairs to tunnel on and off the island. Since the environment can also induce charges on the island, both through controlled operations and unwanted noise, we include a capacitively coupled voltage source in the description. The circuit diagram of a CPB is shown in figure 2.7. Using the standard expressions from sections (2.3) and (2.4), the Lagrangian of the voltage-biased CPB is

$$\mathcal{L}_{CPB} = \frac{1}{2}C_J\dot{\Phi}^2 + \frac{1}{2}C_g\left(\dot{\Phi} - V_g\right)^2 - \left[1 - E_J\cos\left(2\pi\Phi/\Phi_0\right)\right], \tag{2.34}$$

where $\Phi$ is the flux coordinate of the island node. With the canonical momentum (node charge) being $Q = C_J\dot{\Phi} + C_g(\dot{\Phi} - V_g)$, applying the Legendre transformation and neglecting constant terms yields the following Hamiltonian,

$$\mathcal{H}_{CPB} = \frac{1}{2(C_J + C_g)}\left(Q + C_gV_g\right)^2 - E_J\cos\left(2\pi\Phi/\Phi_0\right). \tag{2.35}$$

With $n = -Q/2e$ being the number of Cooper pairs on the island and $n_g = C_gV_g/2e$ the number of Cooper pairs induced by the voltage source, the Hamiltonian (2.35) can be written as

$$\mathcal{H}_{CPB} = 4E_C\left(n - n_g\right)^2 - E_J\cos\phi, \tag{2.36}$$

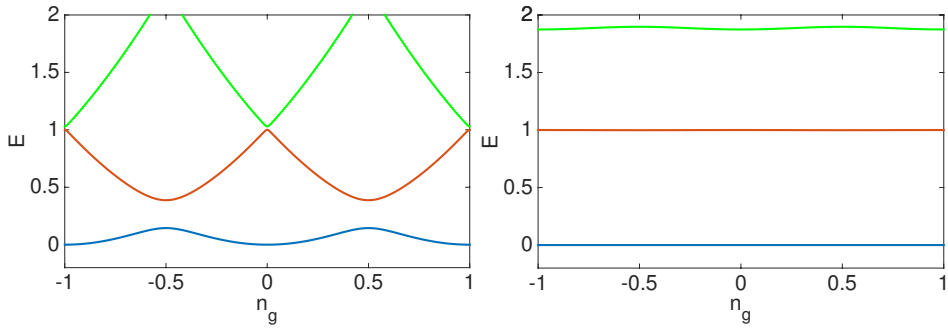


Figure 2.8: The three lowest energy levels of the Cooper pair box as a function of the charge offset $n_g$, for $E_J/E_C = 1$ (left) and $E_J/E_C = 20$ (right). The energy is given in units of the separation between the two lowest states for $n_g = 0$.

where $E_C = e^2/2(C_J + C_g)$ is referred to as the *charging energy*.

Stepping to a quantum description, we use the Cooper pair number $n$ and the phase $\phi$ as canonical variables[1], instead of the charge and the flux. The commutation relation (2.4) implies $[n, \phi] = i$ from which we, using the Baker-Hausdorff lemma [91], can derive

$$[e^{i\phi}, n] = e^{i\phi}. \tag{2.37}$$

The Hamiltonian (2.36) can be projected onto the eigenbasis $|n\rangle$ of the Cooper pair number operator $n$. Noting that the commutation relation (2.37) implies $e^{\pm i\phi}|n\rangle = |n \mp 1\rangle$, we obtain

$$\mathcal{H}_{CPB} = \sum_n \left( 4E_C(n - n_g)^2 |n\rangle\langle n| - \frac{E_J}{2}\left(|n-1\rangle\langle n| + |n+1\rangle\langle n|\right)\right). \tag{2.38}$$

The spectrum of (2.38) depends on the designable parameters $E_J$ and $E_C$, as well as the charge offset $n_g$. For $E_C \gg E_J$, the CPB is said to be operated in the charge regime. Here, the charge on the island is well-defined and the eigenstates of the CPB are close to the Cooper pair number eigenstates $|n\rangle$. This is the so-called *charge qubit*. For $E_J \gg E_C$, the CPB is said to be operated in the phase regime. Here, the phase is well-defined, with correspondingly large charge fluctuations. This is the so-called *transmon*.

[1]The operator $\phi$ is to be understood simply as a rescaled flux operator, not a proper quantum phase operator.

In figure 2.8 we plot the three lowest energy levels as a function of $n_g$ for two different cases. With $E_J/E_C = 1$, choosing the voltage bias so that $n_g = 1/2$ makes the two lowest states well separated from the higher energy levels, enabling us to use the system as a qubit. Since the energy levels are highly dependent on $n_g$, however, this qubit is sensitive to charge noise, limiting its coherence times. In the phase regime, we see a decreased dependence on $n_g$, making the transmon much more robust to charge noise. The drawback of increasing $E_J/E_C$ is that the anharmonicity, the difference between the first and second transition energies, decreases. In most cases, however, the anharmonicity is enough for qubit purposes, making the transmon one of the most widely used superconducting qubit designs today. In practice, a DC SQUID is often used instead of a single Josephson junction in order to make $E_J$ tunable. To obtain the small values of $E_C$ required to reach the transmon regime, the SQUID is shunted by a large extra capacitance.

# Chapter 3

# Elements of special relativity

In the early 20th century, Einstein's special theory of relativity (SR) [96] revolutionized our understanding of space and time. Since space and time constitute the background where physical theories take place, SR deeply affects many branches of physics. At the heart of SR lies the concept of *inertial frames*, which are reference frames moving with constant velocities with respect to each other. The theory is based on two basic postulates. The first is the *relativity principle*, which compactly can be stated as "all physical laws are invariant under a change of inertial frame". The second postulate states that the speed of light in vacuum has the same value $c$ in all inertial frames. For a good introductory textbook on special relativity, see [27]. Here, we will only give a brief introduction.

Einstein's two postulates together imply that the temporal and spatial coordinates of two different inertial frames must be related by a *Lorentz transformation*. Let us consider two frames $S$ and $S'$, with coordinates $(t,x,y,x)$ and $(t',x',y',z')$ respectively. For simplicity, we assume that the two frames are in *standard configuration*. This means that the $x$- and $x'$-axes are aligned and that the spatial origin of $S'$ moves along the $x$-axis with velocity $v$, with the origins coinciding at $t = t' = 0$. The Lorentz transformation relating $S$ and $S'$ is then

$$t' = \gamma(v)\left(t - vx/c^2\right), \tag{3.1}$$

$$x' = \gamma(v)\left(x - vt\right), \tag{3.2}$$

with the remaining coordinates transforming trivially. Here,

$$\gamma(v) \equiv \frac{1}{\sqrt{1 - v^2/c^2}} \tag{3.3}$$

is the so-called *Lorentz factor*. It is worth mentioning that, from the relativity principle alone, it follows that $S$ and $S'$ must be related by (3.1)-(3.2) for some nonnegative number $c$. The role of the second postulate is simply to fix the value of $c$ to the speed of light. In the limit $c \to \infty$ we obtain $t' = t$ and $x' = x - vt$, thus retrieving the *Galilean transformation* which is the symmetry transformation of Newtonian mechanics.

From the Lorentz transformation it is apparent that time and space are no longer absolute concepts. Rather, they are interrelated and combine into a single four-dimensional *spacetime* [97], where points are referred to as *events* and trajectories are known as *worldlines*. Spacetime is conveniently described in the language of differential geometry, using the *metric tensor*. To introduce the metric tensor, let us first define the *invariant spacetime interval*

$$ds^2 = -dt^2 + dx^2 + dy^2 + dz^2. \tag{3.4}$$

It is easy to verify that $ds^2$ is invariant under Lorentz transformations.[1] Now, using Einstein's summation convention[2], we can write (3.4) as

$$ds^2 = \eta_{\mu\nu} dx^\mu dx^\nu, \tag{3.5}$$

where $\mu$,$\nu = 0$ corresponds to the temporal coordinate and $\mu, \nu = 1, 2, 3$ to the spatial coordinates. Thus, the metric tensor is given by

$$\eta_{\mu\nu} = \mathrm{diag}(-1,1,1,1). \tag{3.6}$$

This is the so-called *Minkowski metric* of special relativity. The spacetime itself is referred to as *Minkowski space* or simply *flat spacetime*. The Lorentz transformations, taking us from one inertial frame to another, are those that leave $\eta_{\mu\nu}$ invariant. Transforming to a *non-inertial* frame does not preserve the metric, which reflects the fact that physical laws do not generally take the same form in these frames [28].

In general relativity, Minkowski space is generalized to *curved spacetime*, with a more general metric tensor $g_{\mu\nu}$ indicating the presence of

[1] The full class of transformations preserving the interval also includes translations and spatial rotations. Transformations of the type (3.1)-(3.2) are often referred to as *Lorentz boosts*, while Lorentz transformations are understood to include rotations as well. Lorentz transformations and translations are together known as *Poincaré transformations* (or inhomogeneous Lorentz transformations), which specifies the full class of symmetries in special relativity.

[2] Einstein's summation convention is the rule saying that an index appearing twice in a term should be summed over.

gravity. In this case, *all* frames are non-inertial and the physical laws are invariant under *general coordinate transformations*. There is no set of preferred frames like in special relativity. In the following, however, we will focus on special relativity and, more specifically, the phenomenon of time dilation.

## 3.1 Clocks and time dilation

Famous consequences of the Lorentz transformation include *time dilation* and *length contraction*. In this section, we describe time dilation in detail, again making reference to the two inertial frames $S$ and $S'$ in standard configuration. Consider two events at the same spatial point in the $S'$-frame (so that $\Delta x' = 0$), separated by a time delay $\Delta t'$. Using (3.1) and (3.2), we can then show that the time delay between the same events in the $S$-frame is

$$\Delta t = \gamma(v)\Delta t'. \tag{3.7}$$

Thus, since $\gamma(v) > 1$, an observer in the $S$-frame would conclude that a longer time has elapsed between the events than would an observer in the $S'$-frame. This is what is meant by time dilation. It should be emphasized that this phenomenon is completely symmetric between observers in $S$ and $S'$; both observers agree that processes in the *other* system run slower.

Before continuing, let us stop to briefly discuss the concept of time. Even though it is an intuitively obvious quantity, time is rather difficult to define in a stringent way. The best we can do is to define it in terms of how it is measured; time is simply what a clock reads. The next question then becomes, what is a clock? A clock is a device based on some *periodic process*, where the elapsed time can be defined as being proportional to the number of periods. For example, according to today's SI standards, the second is defined as a certain number of periods of the radiation corresponding to the transition between two energy levels of the cesium 133 atom. When discussing different observers, we always assume that each observer has access to a clock. In our example above, we let the two events correspond to consecutive ticks of a clock at rest in $S'$ (and thus moving with velocity $v$ in $S$). The time dilation result (3.7) can then be stated as "moving clocks tick slower". In special relativity, *every* periodic process must behave according to this rule, no matter what actual physical law is responsible for the process.

Time dilation is sometimes popularized in the form of the *twin paradox*, first introduced by Langevin [98]. This is a thought experiment with two twins where one, Alice, stays on Earth while her brother, Rob, embarks on a round trip in space, finally returning to Alice. Since Rob has been in motion, he has aged less due to time dilation and would be younger than Alice at their reunion. Now, a naive application of special relativity would lead to an apparent paradox. According to Rob, Alice has been in motion and due to the symmetry of time dilation she should *also* be the younger of the two. The resolution of this paradox lies of course in the fact that only constant motion is symmetric. In the travel scenario, however, Rob changes inertial frames whereas Alice does not and this breaks the symmetry between them. Indeed, a more careful analysis shows that Rob is younger. In Paper V, we propose a simulation of a "twin paradox scenario" in superconducting circuits.

So far, we have dealt only with clocks moving at constant velocities. In practice, of course, no clock is subject to indefinite constant motion, but has to accelerate at some point. Unlike in the uniform motion case, there is no way to predict how the rate of a generic clock is affected by accelerated motion. Let us consider a pointlike clock moving along an arbitrary path, with velocity $v(t)$ in some arbitrary inertial frame $S$. At each instant, the clock is at rest with respect to some *instantaneous* rest frame. Now, we can define an *ideal clock* [27] as a clock whose rate is affected by its instantaneous velocity only, through the time dilation formula (3.7). The time $\tau$ elapsed on a clock of this type during the interval $(t_i,t_f)$ in $S$ is then given by integrating the infinitesimal version of (3.7) over the path, resulting in

$$\tau = \int_{t_i}^{t_f} \sqrt{1 - \frac{v(t)^2}{c^2}} dt. \tag{3.8}$$

The quantity $\tau$ is usually called the *proper time* of the path. Sometimes, the existence of ideal clocks measuring proper time along their paths is referred to as the *clock postulate*. In reality, however, the rate of an accelerated clock depends on its underlying physical mechanisms. For certain finite-size clocks, as investigated in Paper V, the rate obviously changes in the case of accelerated motion. For decay rates of unstable particles accelerated in storage rings, time dilation according to the ideal clock formula (3.8) has been experimentally verified to high accuracy [99]. As pointed out in [100], however, even these rates must fundamentally be modified due to acceleration.

## 3.2 Acceleration and rigid body motion

Let us now in detail describe acceleration in special relativity. In the following, we assume that the two inertial frames $S$ and $S'$ are in standard configuration and that all motion takes place along the $x$-axis. The Lorentz transformation (3.1)-(3.2) implies that the velocities of a particle in the two frames are related by

$$u' = \frac{u - v}{1 - uv/c^2}, \tag{3.9}$$

with $u = dx/dt$ and $u' = dx'/dt'$. Similarly, accelerations in the two frames are related by

$$a' = \left( \frac{\sqrt{1 - v^2/c^2}}{1 - uv/c^2} \right)^3 a. \tag{3.10}$$

Now, consider the special case where $S'$ is the instantaneous rest frame of the particle, so that $u = v$. The acceleration measured in this frame is known as the *proper acceleration* $\alpha$ and is given by

$$\alpha = \frac{a}{(1 - u^2/c^2)^{3/2}} = \gamma(u)^3 a. \tag{3.11}$$

The proper acceleration is what an observer feels, sitting in an accelerated vehicle. As we will see in section 4.6, observers moving with *constant* proper accelerations are the only non-inertial observers that can meaningfully define particles in quantum field theory. Suppose now that $\alpha$ is constant, in which case we can integrate (3.11) to obtain

$$\alpha t = \frac{u}{\sqrt{1 - u^2/c^2}}, \tag{3.12}$$

where we have used the inital condition $u = 0$ for $t = 0$. Squaring (3.12) and solving for $u$ yields

$$u = \pm \frac{\alpha t}{\sqrt{1 + \frac{\alpha^2 t^2}{c^2}}}, \tag{3.13}$$

and one more integration, with the integration constant set to zero, leads to the result

$$x = \pm \sqrt{c^2 t^2 + \frac{c^4}{\alpha^2}}. \tag{3.14}$$

Equation (3.14) describes hyperbolas in the $xt$-plane (see figure 3.1) and for this reason, motion with constant proper acceleration is known as *hyperbolic motion*. This is the relativistic counterpart of parabolic motion $x = \pm \alpha t^2/2$ in Newtonian mechanics.

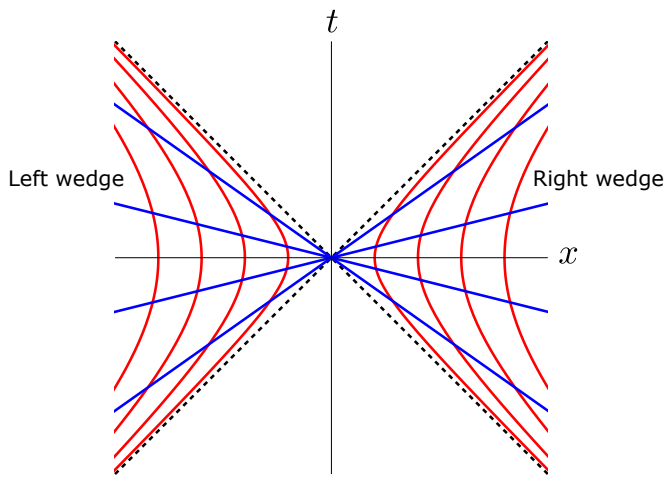


Figure 3.1: Diagram of the Rindler coordinates. The red hyperbolas are curves of constant Rindler position $\chi$, corresponding to uniformly accelerated observers. The blue lines are surfaces of constant Rindler time $\eta$. The dashed lines correspond to lightlike trajectories and are horizons for the Rindler observers.

### 3.2.1 Rindler coordinates

A convenient way to parametrize hyperbolic worldlines is to use the *Rindler coordinates* $(\eta, \chi)$, defined by

$$x = \chi \cosh(\beta\eta/c), \tag{3.15}$$

$$t = \frac{\chi}{c} \sinh(\beta\eta/c), \tag{3.16}$$

or inverted

$$\chi = \sqrt{x^2 - c^2t^2}, \tag{3.17}$$

$$\eta = \frac{c}{\beta} \operatorname{arctanh}(ct/x), \tag{3.18}$$

where $\beta$ is an arbitrary transformation parameter with dimensions of acceleration. Now, (3.17) implies that an observer at constant Rindler position $\chi$ is moving hyperbolically with proper acceleration $c^2/\chi$ in the positive $x$-direction. Moreover, the surfaces of constant Rindler time are straight lines through the origin, as seen in figure 3.1. Writing the metric in Rindler coordinates, we have

$$ds^2 = -\frac{\beta^2\chi^2}{c^2}d\eta^2 + d\chi^2, \tag{3.19}$$

from which we clearly can see that the $\chi$-coordinate measures distance along a surface of constant Rindler time. Moreover, (3.19) looks exactly like the metric of a curved spacetime, with a gravitational field strength proportional to $1/\chi$.

The Rindler coordinates defined as in (3.15)-(3.16) describe observers accelerating in the positive $x$-direction, and the corresponding region of spacetime is known as the *right Rindler wedge* (see figure 3.1). Likewise, the *left Rindler wedge* describes observers accelerating in the negative $x$-direction. In this case, the Rindler coordinates are defined with a different sign in (3.15).

As we will see in section 4.6 when solving the Klein-Gordon equation, it is sometimes convenient to use a different parametrization $\xi$ of the Rindler position, defined by

$$\xi = \frac{c^2}{\beta} \ln\left(\beta\chi/c^2\right). \tag{3.20}$$

### 3.2.2 Relativistic rigid body motion

In Newtonian mechanics, a rigid body is defined as a body where two given points are always at the same distance from each other. In other words, a rigid body is not deformed and is not subject to any strains or stresses. Stepping to relativity this concept becomes problematic, since the distance between any two points is observer-dependent. Thus, we define rigidity by requiring that the distance from any given point A to any other point B on the body is constant in the *instantaneous rest frame* of A. This condition is known as *Born rigidity* [101]. Clearly, a body satisfying Born rigidity is not subject to strains or stresses.

In Newtonian mechanics, a rigid body can move in any fashion. In relativity, this is not the case and Born rigidity is a property of the type of motion rather than of the body itself. Let us start by considering inertial motion. Even though the shape of a body in general is distorted for a moving observer due to length contraction along the direction of motion, it is preserved in the body's rest frame and the motion is rigid.

Next, let us consider the case of uniform acceleration. More specifically, we consider a one-dimensional rod accelerating along the direction of its extension. For the Born rigidity condition to be satisfied, the entire rod must instantaneously come to rest in some inertial frame $S$ at any given instant. The length $L$ as measured in this frame, known as the *proper length*, must be constant throughout the motion. Suppose now that each

point on the rod accelerates with the same proper acceleration. As seen in $S$, this means that the length is preserved while the rod still gains speed. Thus, it is longer than the proper length in its new rest frame and the Born rigidity cannot be satisfied. Instead, the rod must shrink with respect to a fixed arbitrary inertial frame as it gains speed.

Now, suppose that one point on the rod moves hyperbolically. What should the trajectories of the remaining points look like for the proper length to be preserved? We have seen that the $\chi$-coordinate as defined in (3.17) measures distance for the uniformly accelerated observer. Thus, in order for the distance between any two points to be preserved, the difference between their $\chi$-values must be constant. This means that, if one point is moving hyperbolically, so must all the other points, but with different proper accelerations. To be more specific, suppose that the center of the rod moves with proper acceleration $a$, corresponding to the Rindler position $\chi = c^2/a$. If a point at a distance $L$ from the center accelerates with $a_L$, we then have

$$\pm\left(\frac{c^2}{a_L} - \frac{c^2}{a}\right) = L, \tag{3.21}$$

where the plus (minus) sign is for points towards the front (rear) of the rod. Now, (3.21) implies

$$a_L = \frac{a}{1 \pm \frac{aL}{c^2}}, \tag{3.22}$$

and we see that the proper acceleration steadily increases from the front to the rear. It is interesting to note that (3.22) diverges as $L \to c^2/a$. Thus for a given acceleration $a$ at the center of the cavity, there is a limitation to how long the rod can be for the rear end to "keep up" with the rest of the body.

As seen from (3.22), a force gradient applied all along the length of the rod is required to accelerate it from rest while preserving its proper length. Applying a force to a single point necessarily breaks the rigidity due to the finite travel time of information along the rod. After an initial relaxation time, though, it is possible that the rod starts moving rigidly due to internal forces, if the applied force is constant [102]. More generally, the proper length cannot be preserved for time-dependent accelerations unless a pre-programmed force is applied all along the length. For small enough changes in acceleration, however, rigid motion is a good approximation. In Papers V and VI, we consider a Klein-Gordon field in a rigidly moving cavity.

# Chapter 4

# Quantum field theory and quantum optics

As the name suggests, quantum field theory (QFT) [37] concerns the application of quantum mechanics to *fields*. Currently, our most fundamental theories of elementary particles are formulated in the framework of QFT. Here, the field is the fundamental concept whereas particles can be derived as *excitations* of the field. Moreover, these theories are Lorentz invariant, successfully unifying special relativity and quantum mechanics.

The quantum field theory describing the electromagnetic (EM) field and its interaction with matter is *quantum electrodynamics* (QED). In QED, both the EM field and the matter is described by relativistic quantum fields. The electromagnetic part is described by a vector field with photons as excitations and the matter is described by spinor fields with fermionic particles (such as electrons) as excitations. This treatment is required to treat processes in high-energy physics, such as scattering in particle accelerators. In most experiments in other areas, however, the matter can be treated as *atoms* described by standard non-relativistic quantum mechanics, while the full relativistic quantum field description is kept for the EM field. This is the regime of *quantum optics* [103, 104].

In many cases in quantum optics, the electromagnetic vector field is plane polarized. Under these circumstances, the polarization degree of freedom is unimportant and the EM field can be effectively treated as a *scalar field*. As we saw in section 2.6, this approach works particularly well for the field in a coplanar waveguide, where the geometry constrains the polarization to one dimension.

In section 4.1, we quantize the massless Klein-Gordon field, mainly following [26], and in section 4.2 we discuss its interaction with atoms, following [104]. In the three subsequent sections, different states of the field are discussed in the discrete-mode and continuous-mode cases. In section 4.3, we introduce the important subclass of Gaussian states [105, 106] for discrete modes. In section 4.4 we discuss single-mode states, following [103] and [104], and in section 4.5 continuous-mode states [104]. Finally, in sections 4.6 and 4.7 we quantize the field in noninertial frames [38] and introduce Bogoliubov transformations as a tool to change frames.

## 4.1 Klein-Gordon theory

As explained above, a plane polarized electromagnetic field propagating along a single axis can be described by a massless scalar field $\phi(t,x)$ in 1+1-dimensional Minkowski space. As a consequence of Maxwell's equations, this field obeys the massless Klein-Gordon equation

$$\left(\partial_t^2 - c^2\partial_x^2\right)\phi(t,x) = 0. \tag{4.1}$$

We saw in section 2.6 that this is also the equation satisfied by the flux field in a coplanar waveguide.

The wave equation (4.1) has a general solution of the form

$$\phi(t,x) = f\left(x + ct\right) + g\left(x - ct\right), \tag{4.2}$$

corresponding to left- and right-propagating waves. We can expand these in terms of plane wave solutions

$$\phi_k(t,x) = A_k e^{-i(\omega_k t - kx)}, \tag{4.3}$$

with the dispersion relation $|k| = \omega_k/c$. Together with their complex conjugates, the plane waves in (4.3) constitute a complete set of solutions to (4.1) and we can write

$$\phi(t,x) = \int_{-\infty}^{\infty} dk\left[a_k\phi_k(t,x) + c.c.\right], \tag{4.4}$$

for some complex coefficients $a_k$. The normalization factor $A_k$ is chosen so that (4.3) is normalized with respect to the Lorentz invariant *Klein-Gordon inner product* [26]

$$(\phi_1,\phi_2) = -i\int dx\left(\phi_1\partial_t\phi_2^* - \phi_2^*\partial_t\phi_1\right), \tag{4.5}$$

according to

$$(\phi_k,\phi_{k'}) = \delta\left(k-k'\right), \tag{4.6}$$
$$(\phi_k^*,\phi_{k'}^*) = -\delta\left(k-k'\right). \tag{4.7}$$

Note that the complex conjugates $\phi_k^*$ have negative norm. In a single-particle description, where the norms are interpreted as probabilities, this is problematic. Thus, a multi-particle theory is required to successfully unite quantum mechanics and special relativity, as we will see below. We note that, since we have

$$i\partial_t\phi_k(t,x) = \omega_k\phi(t,x) \tag{4.8}$$
$$i\partial_t\phi_k^*(t,x) = -\omega_k\phi^*(t,x) \tag{4.9}$$

the basis functions, or *mode functions*, naturally can be split up into sets of positive and negative frequencies. It is easy to check that this classification is Lorentz invariant, so that all inertial observers agree on which solutions are of positive or negative frequency.

The quantization procedure of any field $\phi(t,x)$ involves writing down the Lagrangian density $\mathcal{L}$ in terms of $\phi(t,x)$ and its derivatives and finding the conjugate momentum $\Pi(t,x) = \partial\mathcal{L}/\partial\dot{\phi}$. Next, $\phi(t,x)$ and $\Pi(t,x)$ are promoted to operators obeying the equal time canonical commutation relation

$$[\phi(t,x),\Pi(t,x')] = i\hbar\delta(x-x'). \tag{4.10}$$

For the free Klein-Gordon field, the canonical momentum is simply $\Pi(t,x) = \partial_t\phi(t,x)$. In the case of the flux field in a CPW, it corresponds to a charge density field, as we saw in section 2.6. The promotion of $\phi(t,x)$ to an operator has the consequence that the coefficients $a_k$ in (4.4) become operators as well, and imposing (4.10) implies

$$\left[a_k, a_{k'}^\dagger\right] = \delta(k-k'), \tag{4.11}$$

with all the remaining commutators vanishing. These are the usual harmonic oscillator commutation relations [91], with $a_k$ and $a_k^\dagger$ being annihilation and creation operators, respectively. The Klein-Gordon field can thus be thought of as a continuum of harmonic oscillators. In terms of $a_k$ and $a_k^\dagger$, the Hamiltonian becomes

$$H = \hbar\int_{-\infty}^{\infty} dk\omega_k\left[a_k^\dagger a_k + \frac{1}{2}\delta(0)\right]. \tag{4.12}$$

### 4.1.1 The vacuum

To find the spectrum of the Hamiltonian (4.12), we require that the ground state $|0\rangle$, known as the *vacuum*, satisfies

$$a_k |0\rangle = 0, \quad \forall k. \tag{4.13}$$

The vacuum is understood to be the zero-particle state. It is not, however, a state of zero energy. As can be seen from (4.12), the zero-point energy of each oscillator mode contributes to make the total energy infinite. These so-called vacuum fluctuations can be viewed as photons of all possibles energies constantly being created and annihilated.

The infinity of the vacuum is usually handled by arguing that only energy differences are measurable, so that the ground state energy can arbitrarily be shifted. The vacuum fluctuations do, however, give rise to observable phenomena in many cases when the field interacts with external systems. In quantum optics, the fluctuations give rise to a renormalization of the atomic energy levels known as the *Lamb shift* [107, 108] and are also responsible for the process of spontaneous emission [109].

Other observable vacuum phenomena occur when boundary conditions for the field are imposed. Placing two perfectly conducting plates close to each other will result in an attractive force between them due to radiation pressure, since the mode density is lower between the plates than outside the plates. This is known as the (static) *Casimir effect* [110] and has been observed in several contexts [111–113]. A related phenomenon is the *dynamical Casimir effect* (DCE) [74] . This is the creation of photon pairs from the vacuum when the boundary conditions, represented by mirrors, are time-dependent. The first prediction of the DCE was done for a field between two mirrors [74] and was later generalized to the case of a single mirror oscillating in open space [114]. For a mirror oscillating sinusoidally, the photon generation rate is given by [115]

$$N = \frac{\Omega}{6\pi} \left( \frac{v_{\max}}{c} \right)^2, \tag{4.14}$$

where $\Omega$ is the oscillation frequency and $v_{\max}$ is the maximal velocity of the mirror. We see from (4.14) that, for the photon production rate to be significant, the mirror must reach velocities that are not too small compared to the speed of light. Due to the obvious difficulties in reaching this regime, the DCE eluded experimental observation for many years.

As mentioned in section 2.6.1, however, it was in 2011 finally observed in a coplanar waveguide with a SQUID generating the time-dependent boundary condition [39]. Studying the DCE in superconducting circuits is not only of fundamental interest. The produced photons are entangled [116] and in [117], it was proposed that the effect may be exploited to generate entanglement between artificial atoms.

The DCE can be viewed as parametric amplification of the vacuum [118]. Recently, a different type of experiment involving the vacuum was performed where, by using short laser pulses, the vacuum fluctuations could be sampled directly in the time-domain without amplification [119].

### 4.1.2 Fock space

Having defined the ground state, the remaining states in the spectrum are formed by acting on $|0\rangle$ with the creation operators. An arbitrary eigenstate of (4.12) is given by

$$a^\dagger_{k_1} a^\dagger_{k_2} ... a^\dagger_{k_{N-1}} a^\dagger_{k_N} |0\rangle \,, \tag{4.15}$$

where the operator $a^\dagger_k$ creates a particle with wavevector $k$ and energy $\hbar\omega_k = \hbar c|k|$. The space spanned by these states is known as the *Fock space*. For each mode, specified by the wavevector $k$, there is an orthonormal basis of particle number eigenstates,

$$|n_k\rangle = \frac{1}{\sqrt{n!}} \left(a^\dagger_k\right)^n |0\rangle \,, \tag{4.16}$$

known as the *Fock basis*. The Fock bases for all modes together span the entire Fock space.

The classification of mode functions in terms of positive and negative frequencies is essential in the construction of the Fock space and thus in the definition of particles. As seen in the field expansion (4.4), positive (negative) frequencies are associated with annihilation (creation) operators. If these different types of operators are not distinguishable, we cannot construct the Fock space. The quantization procedure above was carried out in an inertial frame, and we saw that the mode functions can be split according to (4.8)-(4.9). In an arbitrary noninertial frame or curved spacetime, however, a similar classification of mode functions is not possible and the notion of a particle as defined in QFT is lost. In section 4.6, we discuss under what conditions the construction of the Fock space is possible.

In the expansion (4.4), negative (positive) $k$ corresponds to waves propagating to the left (right). It is sometimes more convenient to split $\phi(t,x)$ into a left- and a right-moving part and integrate over $\omega$ instead of $k$. In the specific case of the flux field in section 2.6, the normalized left- and right-moving field operators are given by

$$\Phi_L(t,x) = \sqrt{\frac{\hbar Z_0}{4\pi}} \int_0^\infty \frac{d\omega}{\sqrt{\omega}} \left[ a_\omega^L e^{-i(\omega t + k_\omega x)} + \text{h.c.} \right], \tag{4.17}$$

$$\Phi_R(t,x) = \sqrt{\frac{\hbar Z_0}{4\pi}} \int_0^\infty \frac{d\omega}{\sqrt{\omega}} \left[ a_\omega^R e^{-i(\omega t - k_\omega x)} + \text{h.c.} \right], \tag{4.18}$$

where $a_\omega^L$ ($a_\omega^R$) is understood to annihilate a left- (right-) moving particle with frequency $\omega$. $Z_0 = \sqrt{L_0/C_0}$ is the *characteristic impedance* of the transmission line.

### 4.1.3 Cavity modes

When confining the field to a cavity, the left- and right-propagating solutions combine into standing waves and the mode structure becomes discrete. A cavity constructed out of two perfectly conducting mirrors can be modeled by imposing two Dirichlet boundary conditions $\phi(t,x_l) = \phi(t,x_r) = 0$, with $x_r - x_l = L > 0$. In this case, a complete set of solutions to the Klein-Gordon equation is given by

$$u_n(t,x) = \frac{1}{\sqrt{n\pi}} \sin\left(k_n(x - x_l)\right) e^{-i\omega_n t}, \quad n = 1,2,3... \tag{4.19}$$

with $\omega_n = \pi n c/L$ and $k_n = \omega_n/c$. The mode functions (4.19) and their complex conjugates satisfy

$$(u_n,u_{n'}) = \delta_{nn'} \tag{4.20}$$

$$(u_n^*,u_{n'}^*) = -\delta_{nn'}, \tag{4.21}$$

with the inner product defined as in (4.5). Analogously to (4.4), the field operator can be expanded as

$$\phi(t,x) = \sum_{n=1}^{\infty} \left( a_n u_n(t,x) + a_n^\dagger u_n^*(t,x) \right), \tag{4.22}$$

with

$$\left[ a_m, a_n^\dagger \right] = \delta_{mn}. \tag{4.23}$$

## 4.2 Light-matter interaction

In quantum optics, light-matter interaction is represented by atoms coupled to the electromagnetic field. When the size of the atom is much smaller than the wavelength of the field, as is usually the case, the interaction can be treated as pointlike. More specifically, only the electric dipole term in the multipole expansions of the electric and magnetic fields is kept. This is known as the *electric dipole approximation* [104]. The interaction Hamiltonian is of the form

$$H_{ED} = e\vec{D} \cdot \vec{E}, \tag{4.24}$$

where $\vec{D}$ is the dipole moment operator of the atom and $\vec{E}$ is the electric field operator. By confining photons in cavities along one or several directions, the electric field per photon becomes stronger. Since the dipole interaction is proportional to the electric field, the confinement increases the coupling strength. This is done in cavity QED to study light-matter interactions at the quantum level.

In this thesis, our interest lies in atoms interacting with propagating photons. Natural atoms in free space radiate in all directions and couple to light propagating in three dimensions. We are, however, interested in coplanar waveguides, where the field propagates in one dimension only. In these systems, there is good confinement of the electric field in the transverse directions, allowing the coupling to be strong even in the absence of a cavity. Moreover, since the field can only be scattered in one dimension, stronger interference effects occur compared to the 3D case.

Consider now a field propagating along a single axis and with a fixed polarization, quantized in a volume that is of infinite extent along its propagation axis and has a cross sectional area $A$. In this particular case, (4.24) becomes [104]

$$H_{ED} = i\hbar\sqrt{\frac{\alpha}{A}}\int_0^\infty d\omega\sqrt{\omega}\left[a_\omega - a_\omega^\dagger\right]\sum_{mn} D_{mn}\left|m\right\rangle\left\langle n\right|, \tag{4.25}$$

where $\alpha \approx 1/137$ is the fine-structure constant and $D_{mn}$ the transition dipole moment between the atomic eigenstates $|m\rangle$ and $|n\rangle$. It is clear from the $1/\sqrt{A}$-factor in (4.25) that the coupling strength can be increased by tight confinement of the field.

In a CPW, the distance between the center conductor and the ground planes is typically in the micrometer range, resulting in a good confinement. Moreover, the effective dipole moment of an artificial atom is a

designable parameter. These two facts together enable us to strongly couple an artificial atom to propagating photons [53–55].

As stated above, natural and artificial atoms are usually treated as pointlike objects in quantum optics. There is, however, recent work on *giant atoms* [120], which can be experimentally realized in hybrid systems where a transmon is coupled to surface acoustic waves [121].

## 4.3 Gaussian states

In many quantum optics setups, the field is confined to a cavity and the mode-structure is discrete. Often, only one mode is relevant for the experiment, but in some cases several modes are involved. In this section, we introduce the important subclass of *Gaussian states* [105, 106] in the general multimode case. As we will see later, many of the states of importance in quantum optics experiments are Gaussian. Moreover, the Gaussian character of a state is preserved under the action of a unitary transformation $U = e^{-iH}$ generated by a Hamiltonian $H$ which is at most quadratic in the field operators [105]. In the Heisenberg picture, this corresponds to linear transformations of the ladder operators [106],

$$a_n \to \sum_n \left( A_{mn} a_n - B^*_{mn} a^\dagger_n \right) + \alpha_m, \tag{4.26}$$

where unitarity constrains the coefficients to satisfy

$$\sum_k \left( A_{mk} A^*_{nk} - B_{mk} B^*_{nk} \right) = \delta_{ij}, \tag{4.27}$$

$$\sum_k \left( A_{mk} B_{nk} - B_{mk} A_{nk} \right) = 0. \tag{4.28}$$

Many common processes in quantum optics, such as beam-splitting and parametric down-conversion, belong to this category.

In addition to being preserved under the above class of transformations, the Gaussian character of a state is also preserved when tracing out modes. In other words, after tracing out an arbitrary number of modes from a multimode Gaussian state, the reduced state is still Gaussian [122]. In section 4.4, we specialize to single-mode theory and describe the most important states in more detail, Gaussian as well as non-Gaussian.

To introduce Gaussian states, let us begin by defining the *quadrature operators*

$$X_{2n-1} = \frac{1}{2}\left(a_n + a_n^\dagger\right), \tag{4.29}$$

$$X_{2n} = -\frac{i}{2}\left(a_n - a_n^\dagger\right). \tag{4.30}$$

These operators, being the the normalized positions and momenta of the harmonic oscillators corresponding to the field modes, span what is known as the *phase space*. In phase space, a complete description of any state is given by one of several *quasi-probability distributions*, such as the Wigner function. An arbitrary $N$-mode state is thus represented by a function defined on a $2N$-dimensional space [106]. Without delving too deep into the matter, we define the Gaussian states to be those with quasi-probability distributions of Gaussian form. It follows that a Gaussian state is completely described by the first and second moments of the quadrature operators, allowing us to greatly simplify the description of the states. Instead of a full density operator treatment, we can use the *covariance matrix formalism*.

We describe the first and second moments of the field by the vector

$$R = (\langle X_1\rangle, \langle X_2\rangle, ...) \tag{4.31}$$

and the *covariance matrix* $\sigma$, with the elements defined by[1]

$$\sigma_{mn} = \frac{1}{2}\langle X_m X_n + X_n X_m\rangle - \langle X_m\rangle\langle X_n\rangle. \tag{4.32}$$

In the covariance matrix formalism, Gaussian-preserving unitary transformations on the Hilbert space are represented by *symplectic* transformations on $R$ and $\sigma$ [105]. These can be written as

$$R \rightarrow SR + d, \tag{4.33}$$

$$\sigma \rightarrow S\sigma S^T, \tag{4.34}$$

where $d$ is a real vector and $S$ is a matrix satisfying

$$S\Omega S^T = \Omega. \tag{4.35}$$

[1] In literature, the definition of the covariance matrix sometimes differ by a factor of 2.

Here, $\Omega$ is the *symplectic form*, defined by

$$[X_m,X_n] = i\Omega_{mn}. \tag{4.36}$$

In the $N$-mode case, unitary operations on the infinite dimensional Fock space can thus be described by $2N \times 2N$-matrices. Another operation which is greatly simplified in the covariance matrix formalism is taking the partial trace over the subsystem corresponding to a certain mode. To find the covariance matrix for the reduced state, the rows and columns corresponding to the traced out mode are simply deleted from the original matrix [26].

## 4.4 Single-mode states

In many experiments in quantum optics, only a single cavity mode is of relevance. In this section, we describe a few of the most important single-mode states. We can conveniently visualize a state in phase space by letting the horizontal and vertical axes represent the $X_1$- and $X_2$-quadrature, respectively. A state is then pictured by a region in phase space, whose location represents the expectation values $\langle X_i \rangle$ and whose shape in some qualitative sense represents the variances

$$\Delta X_i = \sqrt{\langle X_i^2 \rangle - \langle X_i \rangle^2}. \tag{4.37}$$

Note that the mean square deviations $(\Delta X_i)^2$ of the quadrature operators are the diagonal elements of the covariance matrix (4.32). Often, it is also useful to calculate the mean and the variance of the photon number operator $\hat{n} = a^\dagger a$.

### 4.4.1 Fock states

Let us start with the eigenstates $|n\rangle$ of the photon number operator $\hat{n}$, known as *Fock states*. For these states we have $\langle \hat{n} \rangle = n$ and $\Delta \hat{n} = 0$ and as we saw in section 4.1, they constitute a complete basis for the Fock space. For the quadrature operators we have $\langle X_1 \rangle = \langle X_2 \rangle = 0$, and thus the expectation value of the field is always zero for a Fock state, no matter the number of photons. This means that the phase is completely undefined. Since a classical field solution corresponds to a wave with a well-defined

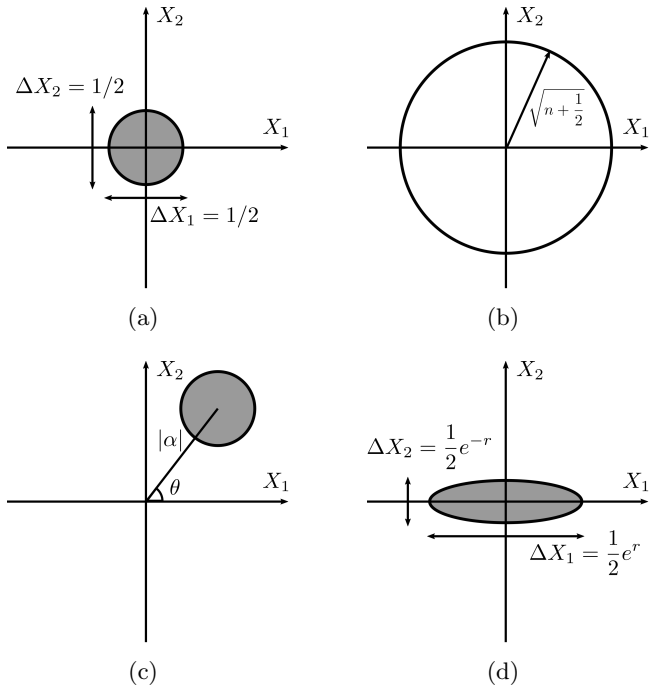


Figure 4.1: Phase space representations of four different single-mode states. (a) The vacuum is represented by a disc centered at the origin, indicating equal fluctuations in the quadratures. (b) The Fock state $|n\rangle$ is represented by a circle, indicating that the photon number is definite and the phase is undetermined. (c) A coherent state is represented by a circle displaced by $\alpha = |\alpha|e^{i\theta}$. (d) The squeezed vacuum with squeezing parameter $r$ is represented by an ellipse with major (minor) axis $e^r/2$ ($e^{-r}/2$). Here, the squeezing angle is $\phi = 0$.

phase, the Fock states are in some sense the most "quantum mechanical" states. The quadrature variances are

$$\Delta X_1 = \Delta X_2 = \sqrt{\frac{1}{2}\left(n + \frac{1}{2}\right)}. \tag{4.38}$$

In the special case of the vacuum, with $n = 0$, (4.38) becomes $\Delta X_1 = \Delta X_2 = 1/2$. These are the vacuum fluctuations discussed in section 4.1.1. Figure 4.1(a) and 4.1(b) shows the phase space representation of the vacuum and a Fock state with $n > 0$, respectively. With the exception of the vacuum, the Fock states are not Gaussian.

### 4.4.2 Coherent states

In section 4.4.1, we saw that the properties of Fock states are far from those of classical fields, even in the limit of many photons. The quantum mechanical states being "most classical" are instead the *coherent states* [123], loosely speaking being classical fields with vacuum fluctuations. These are to a good approximation the states generated by lasers or microwave generators and are thus very commonly used as input in quantum optics and circuit QED experiments. A coherent state is the simplest example of a Gaussian state.

The coherent states are defined as eigenstates of the annihilation operator,

$$a\left|\alpha\right\rangle = \alpha\left|\alpha\right\rangle, \tag{4.39}$$

where the eigenvalue $\alpha$ is a complex number. Correspondingly, the field operator expectation values look exactly like classical field solutions, while the variances are equal to those of the vacuum. The mean number of photons is $\langle\hat{n}\rangle = |\alpha|^2$ and the variance is easily seen to be $\Delta\hat{n} = |\alpha|$, giving us the fractional uncertainty

$$\frac{\Delta\hat{n}}{\langle\hat{n}\rangle} = \frac{1}{\sqrt{\langle\hat{n}\rangle}}. \tag{4.40}$$

Thus, in the limit of large photon numbers, the coherent state really approaches a classical wave.

Since the quadrature variances of the coherent state are the same as those of the vacuum, the state can be represented by a circle in phase space. The first moments, however, are now nonzero which means that the circle is displaced from the origin, as seen in figure 4.1(c). A coherent state can be obtained from the vacuum as

$$\left|\alpha\right\rangle = D(\alpha)\left|0\right\rangle, \tag{4.41}$$

where

$$D(\alpha) = e^{\left(\alpha a^\dagger - \alpha^* a\right)} \tag{4.42}$$

for obvious reasons is known as the *displacement operator*.

In the Fock basis, the expansion of a coherent state reads

$$\left|\alpha\right\rangle = e^{-\frac{1}{2}|\alpha|^2}\sum_{n=0}^{\infty}\frac{\alpha^n}{\sqrt{n!}}\left|n\right\rangle. \tag{4.43}$$

From (4.43) we can compute the probability $P(n)$ of finding $n$ photons,

$$P(n) = |\langle n|\alpha\rangle|^2 = e^{-\langle\hat{n}\rangle}\frac{\langle\hat{n}\rangle^n}{n!}, \tag{4.44}$$

which we recognize as a *Poissonian distribution*. This distribution arises for processes where the probability for an event is independent of earlier events. In other words, light from a source where the photon emission events are independent from each other has a Poissonian photon number distribution. This is very different from the light emitted from a single atom, as we will see in section 4.5.1.

### 4.4.3 Thermal states

All single-mode states we have considered so far have been pure states. We will now describe the simplest example of a mixed Gaussian state; the thermal state. Thermal states arise when the field is in thermal equilibrium with a heat bath of fixed temperature $T$. In many experiments, the noise background can to a good approximation be considered thermal.

Using statistical mechanics, it is easy to prove that the density operator of a thermal state can be written as

$$\rho_{th} = \sum_{n=0}^{\infty} P(n)\,|n\rangle\,\langle n|\,, \tag{4.45}$$

where the probability $P(n)$ of finding $n$ photons in the mode (of frequency $\omega$) is given by

$$P(n) = \left(1 - e^{-\hbar\omega/k_BT}\right)e^{-\hbar\omega n/k_BT}, \tag{4.46}$$

and where $k_B$ is Boltzmann's constant. The mean number of photons is

$$\langle\hat{n}\rangle = \mathrm{tr}\,(\hat{n}\rho_{th}) = \frac{1}{e^{\hbar\omega/k_BT} - 1}, \tag{4.47}$$

which is the Bose-Einstein distribution. Using (4.47), we can write (4.46) as

$$P(n) = \frac{\langle\hat{n}\rangle^n}{(1 + \langle\hat{n}\rangle)^{n+1}}. \tag{4.48}$$

For the variance, we obtain

$$\Delta\hat{n} = \sqrt{\langle\hat{n}\rangle + \langle\hat{n}\rangle^2}, \tag{4.49}$$

which means that the variance is always larger than the mean.

### 4.4.4 Single-mode Gaussian states

In section 4.3 we introduced the covariance matrix formalism for arbitrary multimode Gaussian states. In this section, we specialize to arbitrary single-mode Gaussian states and give explicit expressions for the first moments and the covariance matrix in terms of physically relevant quantities. In Paper VI, we investigate how these states are affected by relativistic motion.

It can be shown that the density matrix of an arbitrary single-mode Gaussian state can be decomposed as [122]

$$\rho = R(\theta)D(\alpha)S(\xi)\rho_{th}(n)S^\dagger(\xi)D^\dagger(\alpha)R^\dagger(\theta). \tag{4.50}$$

Here, $\rho_{th}(n)$ is the density operator (4.45) of a thermal state with mean photon number $n$, $D(\alpha)$ is the displacement operator (4.42) and $R(\theta) = e^{i\theta a^\dagger a}$ is the phase rotation operator. The remaining operator $S(\xi) = e^{\frac{1}{2}\left(\xi(a^\dagger)^2 - \xi^* a^2\right)}$, with $\xi \equiv re^{i\phi}$ being a complex number, is known as the (single-mode) *squeezing operator*. To understand this operator, let us investigate its effect on the vacuum. Computing the quadrature variances for the so-called *squeezed vacuum state* $S(\xi)\left|0\right\rangle$ yields

$$\Delta X_1 = \frac{1}{2}\sqrt{e^{-2r}\sin^2(\phi/2) + e^{2r}\cos^2(\phi/2)}, \tag{4.51}$$

$$\Delta X_2 = \frac{1}{2}\sqrt{e^{-2r}\cos^2(\phi/2) + e^{2r}\sin^2(\phi/2)}. \tag{4.52}$$

For $\phi = 0$, (4.51)-(4.52) reduces to $\Delta X_1 = e^r/2$ and $\Delta X_2 = e^{-r}/2$. Thus, we clearly see that the squeezing reduces the fluctuations in one quadrature at the expense of increasing them in the other one. We can represent this state by an ellipse ("squeezed circle") in phase space, as seen in figure 4.1(d). For $\phi \neq 0$, the squeezing takes place along a different axis, with $\phi = \pi$ corresponding to the $X_1$-quadrature. With $\phi$ chosen so that the phase fluctuations decrease, squeezed states can be used to enhance the precision in interferometry devices [124, 125].

Let us now return to the arbitrary single-mode Gaussian state (4.50), "a squeezed, displaced and rotated thermal state", and describe it in the covariance matrix formalism. We can without loss of generality take $\alpha$ to be real, since we include the arbitrary phase rotation $R(\theta)$. The first moments become

$$\langle X_1 \rangle \quad = \quad \alpha\cos\theta, \tag{4.53}$$

$$\langle X_2 \rangle = \alpha \sin\theta \tag{4.54}$$

and the covariance matrix

$$\sigma = \begin{bmatrix} \sigma_{11} & \sigma_{12} \\ \sigma_{21} & \sigma_{22} \end{bmatrix}, \tag{4.55}$$

with [122]

$$\sigma_{11} = \frac{(2n+1)}{4}\left[\cosh(2r) + \sinh(2r)\cos(2\theta+\phi)\right], \tag{4.56}$$

$$\sigma_{22} = \frac{(2n+1)}{4}\left[\cosh(2r) - \sinh(2r)\cos(2\theta+\phi)\right], \tag{4.57}$$

$$\sigma_{12} = \sigma_{21} = \frac{(2n+1)}{4}\left[\sinh(2r)\sin(2\theta+\phi)\right]. \tag{4.58}$$

Finally, we also write down the mean photon number of the state [126],

$$\langle \hat{n} \rangle = \alpha^2 + n + (2n+1)\sinh^2 r. \tag{4.59}$$

## 4.5 Continuous-mode states

In sections 4.3 and 4.4 we described states relevant for cavity-based systems. As we saw in section 1.1, setups with propagating photons in coplanar waveguides are also interesting in many contexts. In these open systems, the mode-structure is continuous and a different formalism is required.

The state in (4.16) is a propagating $n$-photon state with definite energy and momentum. This state, however, has its finite energy completely delocalized in space and time and is of limited use in the description of actual physical situations. In realistic scenarios, more than one mode is excited in the propagating field. In this case, the concept of a photon as a single excitation is not as obvious anymore, since the excitation now is distributed over a range of frequencies. We define a photon number state as

$$|n_\xi\rangle = \frac{1}{\sqrt{n!}}\left(a_\xi^\dagger\right)^n |0\rangle, \tag{4.60}$$

where

$$a_\xi^\dagger = \int d\omega \xi(\omega) a_\omega^\dagger \tag{4.61}$$

is the creation operator for a *photon wavepacket*. Here, $a_\omega^\dagger$ creates an excitation with a definite frequency. In the time-domain, $|n_\xi\rangle$ represents an $n$-photon pulse whose shape is given by the Fourier transform of $\xi(\omega)$. Similarly as in the single-mode case, we can define displacement and squeezing operators in terms of the photon wavepacket operators. In this way, we can describe propagating pulses of coherent or squeezed light.

In many cases, the propagating field can be approximated by a *stationary* beam, which has time-independent fluctuation properties and persists indefinitely. The fact that the mean photon number for such a state is infinite poses no problem. What is important is instead the number of photons *per unit time* or, equivalently, the intensity.

### 4.5.1 Coherence functions

A useful way to characterize the state of a propagating field is through the *coherence functions* [127]. While these can be defined to any order, the first- and second-order functions are of special interest since they can be directly related to measurement results in standard interferometers.

When we are interested in correlation functions involving the field operator at different times but at the same spatial point, we can suppress the $x$-argument and write the positive- and negative-frequency parts as $\phi^+(t)$ and $\phi^-(t)$, respectively. The *degree of first order coherence* is defined as

$$g^{(1)}(t_1,t_2) = \frac{\langle \phi^-(t_1)\phi^+(t_2)\rangle}{\sqrt{\langle \phi^-(t_1)\phi^+(t_1)\rangle\langle \phi^-(t_2)\phi^+(t_2)\rangle}} \tag{4.62}$$

and can straightforwardly be measured as the intensity output in a Mach-Zender interferometer. For stationary fields, (4.62) depends only on $\tau = t_2 - t_1$, and we can write

$$g^{(1)}(\tau) = \frac{\langle \phi^-(t)\phi^+(t+\tau)\rangle}{\langle \phi^-(t)\phi^+(t)\rangle}. \tag{4.63}$$

When $|g^{(1)}(\tau)| = 1$, we say that the field is first-order coherent. This is true for all single-mode states and multimode coherent states. For multimode thermal light, we have $|g^{(1)}(\tau)| < 1$, with $g^{(1)}(\tau) \to 0$ as $\tau \to \infty$. Thus, these fields are incoherent and the field correlations are lost entirely for long delay times.

Experiments involving only first-order coherence can be explained classically. In order to examine the true quantum mechanical properties of

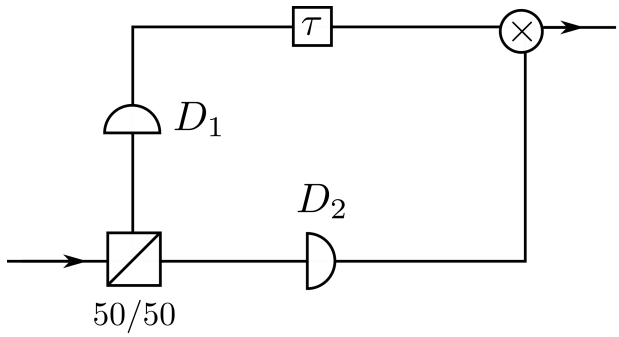


Figure 4.2: Schematic sketch of a Hanbury-Brown-Twiss interferometer. The light is split into two equal parts in a 50/50 beam-splitter. The photodetectors $D_1$ and $D_2$ measure the intensities and, after a relative time delay $\tau$, the two detector outputs are multiplied. In this way, intensity-intensity correlations of the input field as a function of the delay time $\tau$ can be measured. In the microwave regime, there are no photodetectors. Here, the intensity measurements are instead done using linear amplifiers [129].

light, we need to look at the *degree of second-order coherence*, defined in the stationary case as

$$g^{(2)}(\tau) = \frac{\langle \phi^-(t)\phi^-(t+\tau)\phi^+(t+\tau)\phi^+(t)\rangle}{\langle \phi^-(t)\phi^+(t)\rangle^2}. \tag{4.64}$$

While $g^{(1)}(\tau)$ measures field-field correlations, $g^{(2)}(\tau)$ instead measures intensity-intensity correlations, which can be done with a Hanbury-Brown-Twiss interferometer [128] (see figure 4.2). The numerator is proportional to the two-photon coincidence rate at times $t$ and $t+\tau$, or the conditional probability rate of detecting a second photon a time $\tau$ after the first one has been detected.

The degree of second-order coherence as defined in (4.64) can take on a different set of values than its classical counterpart. More specifically, $g^{(2)}(0) < 1$ or $g^{(2)}(0) < g^{(2)}(\tau)$ indicates that the light is *nonclassical*.[2] The two conditions for nonclassicality indicate the presence of *sub-Poissonian* fluctuations and *photon antibunching*, respectively, which are two distinct but often related nonclassical phenomena. In order to understand their meaning, let us first consider the photon number fluctuations of the field.

[2] A stringent definition of nonclassical light can be made in terms of quasi-probability distributions on phase space.

Since the field is stationary, $\hat{n}$ corresponds to the number of photons per unit time.

For a coherent state, it is easy to check that $g^{(2)}(\tau) = 1$ and it is thus *second-order coherent*.[3] As we saw in section 4.4.2, the photon number probability distribution for a coherent state is Poissonian, with variance $\Delta\hat{n} = \sqrt{\langle\hat{n}\rangle}$. Now, states with $\Delta\hat{n} < \sqrt{\langle\hat{n}\rangle}$ or $\Delta\hat{n} > \sqrt{\langle\hat{n}\rangle}$ are said to have *sub-Poissonian* or *super-Poissonian* fluctuations, respectively. Rewriting $g^{(2)}(0)$ in terms of the photon number operator, it is easy to see that these two cases correspond to $g^{(2)}(0) < 1$ and $g^{(2)}(0) > 1$. Thus, states with sub-Poissonian fluctuations are nonclassical and examples of these include the Fock states and the squeezed states. For a thermal state, on the other hand, we always have $g^{(2)}(0) = 2$ and the photon number fluctuations are super-Poissonian.

In a coherent state, where the photon number distribution is Poissonian, the photons arrive at completely random times and this is reflected in the fact that $g^{(2)}(\tau)$ is constant. Having detected a photon, the probability rate of detecting a second one is independent of the delay time. For a thermal state, $g^{(2)}(\tau)$ is always a decreasing function of $\tau$, so that $g^{(2)}(0) > g^{(2)}(\tau)$. Thus, the two-photon detection probability is larger for short time-delays, and the photons tend to arrive in pairs. This phenomenon is known as *photon bunching*. The opposite situation occurs for $g^{(2)}(0) < g^{(2)}(\tau)$, when the photons tend to arrive more evenly spaced. This is known as *photon antibunching* and is a nonclassical effect. In Paper I, we investigate the antibunched field reflected off a single artificial atom in a coplanar waveguide.

## 4.6 Non-inertial frames

In section 4.1, we quantized the Klein-Gordon field in an inertial reference frame. As we saw in (4.8)-(4.9), the solution space could be split into sets of positive and negative frequencies, which was essential in the quantization procedure. In this section, we discuss the conditions that must apply for this procedure to be possible in a non-inertial frame. Having done that, we then go on to quantize the field in a *uniformly accelerated frame*, mainly following [26].

Let us start with a more general case; a possibly curved spacetime with metric tensor $g_{\mu\nu}$. A coordinate transformation that preserves the form of

[3] In fact, the state is coherent to all orders, hence its name.

the metric is known as an *isometry* of the spacetime. For infinitesimal transformations

$$x^\mu \to x^\mu + \epsilon\xi^\mu(x), \tag{4.65}$$

it is possible to show [28] that the condition for the transformation to be an isometry is

$$g_{\mu\sigma}(x)\frac{\partial\xi^\sigma(x)}{\partial x^\nu} + g_{\rho\nu}(x)\frac{\partial\xi^\rho(x)}{\partial x^\mu} + \xi^\gamma(x)\partial_\gamma g_{\mu\nu}(x) = 0. \tag{4.66}$$

A vector field $\xi^\mu(x)$ satisfying (4.66) is known as a *Killing vector*. Now, imagine a spacetime trajectory tangented by a Killing vector. For translations along this trajectory, the metric is preserved and we can thus find a coordinate system where the metric is independent of one of the coordinates. If the trajectory corresponds to the world-line of an observer, the Killing vector is timelike. For this observer, the metric becomes time-independent, which means that we can always split the solution set into positive and negative frequency modes. Thus, only observers flowing along timelike Killing vectors can in a meaningful way construct the Fock space of the field.[4]

In 1 + 1-dimensional Minkowski space, (4.66) becomes

$$\partial_x\xi^0 = \partial_t\xi^1, \tag{4.67}$$

which gives us two possibilities. If the derivatives are zero, the entries in the Killing vector are constant, giving us straight lines in Minkowski space. The timelike straight lines are the worldlines of inertial observers. If the derivatives are nonzero the Killing vector is of the form

$$\xi^\mu \propto (x,t). \tag{4.68}$$

This is the tangent vector of a hyperbola, with the equation

$$x^2 - c^2t^2 = const. \tag{4.69}$$

As we saw in section 3.2, (4.69) corresponds to motion with constant proper acceleration. Thus, the uniformly accelerated frames are the only non-inertial frames in Minkowski space where the particle concept survives.

[4] There is a more operational definition of particles in the form of *particle detectors* [130], but we will not consider it here.

To quantize the Klein-Gordon field, we use the Rindler coordinates introduced in (3.15)-(3.16). Redefining the spatial coordinate according to (3.20), the Klein-Gordon equation simply becomes

$$\left(\partial_\eta^2 - c^2\partial_\xi^2\right)\phi\left(\eta,\xi\right) = 0. \tag{4.70}$$

Since (4.70) is of the same form as (4.1), we can proceed with the quantization procedure in exactly the same way as in the inertial frame. By doing this in open space one can derive the *Unruh effect* [81], which is the prediction that an observer accelerating uniformly through the Minkowski vacuum sees a thermal state. Via the equivalence principle, the Unruh effect is closely related to the phenomenon of *Hawking radiation* [83, 84] in black hole spacetimes.

In this thesis, however, we will instead focus on cavity modes. By imposing the Dirichlet boundary conditions $\phi\left(\eta,\xi_l\right) = \phi\left(\eta,\xi_r\right) = 0$, we find in exact analogue to (4.19) the normalized mode functions

$$v_m(\eta,\xi) = \frac{1}{\sqrt{m\pi}}\sin\left(\frac{\Omega_m}{c}(\xi-\xi_l)\right)e^{-i\Omega_m\eta}, \tag{4.71}$$

with $\Omega_m = \pi c m/L'$ and $L' = |\xi_r - \xi_l|$. The field can now be expanded as

$$\phi(\eta,\xi) = \sum_{m=1}^{\infty}\left(b_m v_m(\eta,\xi) + b_m^\dagger v_m^*(\eta,\xi)\right), \tag{4.72}$$

with $[b_m,b_n^\dagger] = \delta_{mn}$.

We saw in section 3.2.2 that a rigidly and uniformly accelerated rod is static in the Rindler coordinates. Thus, (4.71) are the mode functions in a uniformly accelerated rigid cavity. Note, however, that the proper length is not equal to $L'$, but instead $L = |\chi_r - \chi_l|$. The relation between $L$ and $L'$ depends on the acceleration and can be found using (3.20). For a cavity where the midpoint moves with proper acceleration $a$, we obtain

$$L' = \frac{2c^2}{a}\operatorname{arctanh}\left(\frac{aL}{2c^2}\right), \tag{4.73}$$

where we for simplicity have chosen the transformation parameter in (3.15)-(3.16) as $\beta = a$, so that the Rindler time corresponds to the proper time of an observer in the center of the cavity. In Papers V and VI, we use the Rindler quantization to examine the field in a relativistically moving cavity.

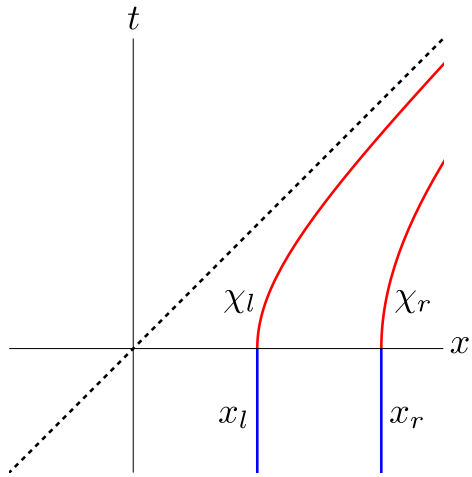


Figure 4.3: A rigid cavity of proper length $L = x_r - x_l$ starts at rest (blue). At time $t = 0$ it starts to accelerate uniformly (red), with a preserved proper length $L = \chi_r - \chi_l$.

## 4.7 Bogoliubov transformations

By using the mode expansion (4.71), we can describe the Klein-Gordon field in a uniformly accelerated cavity, undergoing free time evolution in Rindler time (3.18). This, however, is only true for a cavity that accelerates indefinitely. Consider now instead the situation depicted in figure 4.3, with a cavity of length $L$ starting at rest in some inertial frame with coordinates $(t,x)$. At time $t = 0$, when the cavity starts to accelerate, the field can be expanded both in Minkowski modes and in Rindler modes. We can thus write

$$\sum_{m=1}^{\infty} \left( b_m v_m(\eta,\xi) + b_m^\dagger v_m^*(\eta,\xi) \right) = \sum_{n=1}^{\infty} \left( a_n u_n(t,x) + a_n^\dagger u_n^*(t,x) \right). \quad (4.74)$$

Taking the Klein-Gordon inner product (4.5) with $v_m$ on both sides of (4.74), we arrive at the *Bogoliubov transformation*

$$b_m = \sum_{n=1}^{\infty} \left( \alpha_{mn}^* a_n - \beta_{mn}^* a_n^\dagger \right), \quad (4.75)$$

with $\alpha_{mn} = (v_m,u_n)$ and $\beta_{mn} = (v_m,u_n^*)$ being known as *Bogoliubov coefficients*. These are inner products (4.5) between the Minkowski and Rindler

mode functions, with the integrals being evaluated at $t = 0$. The off-diagonal $\alpha$-coefficients relate the annihilations operators in the two frames and therefore account for *mode-mixing*. The $\beta$-coefficients, on the other hand, relate annihilation and creation operators and thus account for *particle creation*. As long as $\beta_{mn} \neq 0$, the Minkowski and Rindler frames have different vacuum states. The DCE, the Unruh effect and Hawking radiation can all be described by Bogoliubov transformations with nonzero $\beta$-coefficients.

Let us now consider a rigid cavity undergoing a trajectory consisting of segments of inertial motion and uniform acceleration. We can describe the full evolution of the state in this cavity by applying a sequence of Bogoliubov transformations (4.75) and their inverses, with free time-evolution in Minkowski or Rindler coordinates in between [77]. This is exploited when describing the "twin paradox scenario" in Paper V.

Finally, we note that the Bogoliubov transformations take the same form as (4.26), with $\alpha_m = 0$. This means that they map Gaussian states into Gaussian states; a fact that is exploited in Paper VI when we investigate the precision of an accelerated clock. Recall from section 4.3 that a transformation of this type can be represented by a symplectic operation acting on the first moments and the covariance matrix. Explicitly, the symplectic matrix corresponding to the transformation (4.75) is constructed using the $2 \times 2$-blocks [131]

$$\mathcal{M}_{mn} = \begin{pmatrix} \mathrm{Re}(\alpha_{mn} - \beta_{mn}) & \mathrm{Im}(\alpha_{mn} + \beta_{mn}) \\ -\mathrm{Im}(\alpha_{mn} - \beta_{mn}) & \mathrm{Re}(\alpha_{mn} + \beta_{mn}) \end{pmatrix} . \tag{4.76}$$

# Chapter 5

# Open quantum systems

A *closed quantum system* is a system which is totally independent of its surroundings. The dynamics of a closed system is governed by *unitary evolution*, depending only on the system Hamiltonian $H$. In the *Schrödinger picture* the states $|\Psi(t)\rangle$ are time-dependent and obey the Schrödinger equation,

$$i\hbar\frac{d}{dt}|\Psi(t)\rangle = H|\Psi(t)\rangle, \tag{5.1}$$

while the operators $A$ are time-independent. In the *Heisenberg picture*, the operators $A(t)$ are instead time-dependent and obey the Heisenberg equation,

$$i\hbar\frac{dA(t)}{dt} = [A(t), H], \tag{5.2}$$

while the states $|\Psi\rangle$ are time-independent. Equations 5.1 and 5.2 give equivalent descriptions for the dynamics of *pure states*. A generalization of the pure states are the *mixed states*, which are statistical ensembles of pure states. To describe mixed states, we can introduce the density operator $\rho = \sum_i w_i |\psi_i\rangle\langle\psi_i|$, where $w_i$ is the probability for the system to be in the state $|\psi_i\rangle$. For a closed system, the time evolution of the density operator is given by the *Liouville-von Neumann equation*,

$$\frac{d\rho(t)}{dt} = -\frac{i}{\hbar}[H, \rho(t)], \tag{5.3}$$

which of course is equivalent to (5.1) in the special case of pure states.

In reality, no system can be completely isolated from the rest of the world and the only truly closed system is the entire Universe. In some

cases, the influence of the outside world is negligible and the equations for a closed system are valid to a good approximation. Often, however, the influence of some part of the external world called the *environment* is important. Typically, the environment contains far more degrees of freedom than the system of interest and is impossible to describe exactly. This situation is treated in the formalism of *open quantum systems*. One is only interested in the evolution of the system, where the influence of the environment shows up as *noise*.

The density operator of an open quantum system evolves according to a *master equation*, which is a generalization of (5.3). There are also cases where the surroundings carry signals of interest, which can be modified by interaction with the system. In those cases, the master equation is accompanied by *input-output equations*. The main goal of this chapter is to derive a master equation and input-output equations for a quantum optical system.

In many cases, the environment of a quantum system is modeled as a bath of harmonic oscillators linearly coupled to the system. This is known as the *Caldeira-Leggett*-model [132] and works very well in quantum optics, where the system and the environment correspond to an atom coupled to the electromagnetic field. Using this model, we derive input-output equations in section 5.1 and a quantum optical master equation in section 5.2. These derivations largely follow the treatment in [133].

## 5.1 Input-output equations

We consider a system whose free evolution is described by the arbitrary Hamiltonian $H_{\text{sys}}$, coupled to a bath in form of a one-dimensional Klein-Gordon field $\phi(t,x)$ at the end of a semi-infinite open space. This field can represent a real transmission line, like the coplanar waveguide in section 2.6, but can also be used to model dissipation of the system into unknown channels.

The total Hamiltonian can be written as $H = H_{\text{sys}} + H_B + H_{\text{int}}$ where

$$H_B = \frac{1}{2}\int_0^\infty dx \left[\pi(t,x)^2 + c^2\left(\partial_x\phi(t,x)\right)^2\right], \tag{5.4}$$

is the bath Hamiltonian, with $\pi(t,x)$ being the canonical momentum of $\phi(t,x)$. The interaction Hamiltonian is

$$H_{\text{int}} = X\int_0^\infty dx\kappa(x)\dot{\phi}(t,x), \tag{5.5}$$

where $X$ is the system operator that couples to the field. The coupling coefficient $\kappa(x)$ is nonzero only in a small range around $x = 0$.

In contrast to the case of the open transmission line, the left and right moving modes are not independent. Thus, dropping the wavenumber index and the constant terms in (4.12), the bath Hamiltonian can be written as

$$H_{\mathrm{B}} = \hbar \int_0^\infty d\omega\, \omega a_\omega^\dagger a_\omega, \tag{5.6}$$

with

$$\left[a_\omega, a_{\omega'}^\dagger\right] = \delta(\omega - \omega'). \tag{5.7}$$

Similarly, the interaction Hamiltonian becomes

$$H_{\mathrm{int}} = i \int_0^\infty d\omega \kappa(\omega) \sqrt{\frac{\hbar\omega}{2}} \left(a_\omega^\dagger - a_\omega\right) X, \tag{5.8}$$

where $\kappa(\omega)$ is the Fourier transform of the coupling coefficient $\kappa(x)$. We can expand the operator $X$ in eigenoperators of $H_{\mathrm{sys}}$,

$$X = \sum_i \left(X_i^+ + X_i^-\right), \tag{5.9}$$

with

$$\left[H_{\mathrm{sys}}, X_i^\pm\right] = \pm\hbar\omega_i X_i^\pm. \tag{5.10}$$

In the system eigenbasis, $X_i^\pm$ are *raising* and *lowering* operators, with $\omega_i$ being the corresponding transition frequencies.

Let us now consider the case of a system with only one transition frequency $\omega_s$, so that $X = X^+ + X^-$, and use some approximations to simplify the interaction Hamiltonian (5.8). Our first assumption is that the interaction is *weak*, in the sense $H_{\mathrm{int}} \ll H_{\mathrm{sys}}$. This implies that the time dependence of $X^\pm$ is approximately $e^{\pm i\omega_s t}$. In quantum optics, the processes of interest typically occur on a timescale much longer than $1/\omega_s$. On these timescales terms of the type $X^- a(\omega)$, oscillating like $e^{-i(\omega+\omega_s)t}$, average to zero and can be dropped. This is the so-called *rotating wave approximation* (RWA). Moreover, the lower integration limits of (5.6) and (5.8) can without problem formally be extended to $-\infty$, since all the added terms are far off resonance.

Now, employing the above approximations and defining

$$\gamma(\omega) = \kappa(\omega)\sqrt{\omega/2\hbar} \tag{5.11}$$

we can write

$$H_{\rm B} = \hbar \int_{-\infty}^{\infty} d\omega\, \omega a_\omega^\dagger a_\omega, \tag{5.12}$$

$$H_{\rm int} = i\hbar \int_{-\infty}^{\infty} d\omega \gamma(\omega) \left[ a_\omega^\dagger X^- - X^+ a_\omega \right]. \tag{5.13}$$

From these approximate Hamiltonians, we follow [134] to find the input-output equations. Working in the Heisenberg picture, we use (5.2) to obtain

$$\dot{a}_\omega = i\omega a_\omega + \gamma(\omega) X^-, \tag{5.14}$$

$$\dot{b} = -\frac{i}{\hbar}[b,H_{\rm sys}] + \int_{-\infty}^{\infty} d\omega \gamma(\omega) \left[ a_\omega^\dagger \left[b,X^-\right] - \left[b,X^+\right] a_\omega \right], \tag{5.15}$$

where $b$ is an arbitrary operator of the system. An operator without the time argument explicitly written out is understood to be a Heisenberg operator at time $t$. Now, solving (5.14) and inserting the solution into (5.15) yields

$$\begin{aligned} \dot{b} &= -\frac{i}{\hbar}[b,H_{\rm sys}] \\ &+ \int_{-\infty}^{\infty} d\omega \gamma(\omega) \left[ e^{i\omega(t-t_0)} a_\omega^\dagger(t_0) \left[b,X^-\right] - \left[b,X^+\right] e^{-i\omega(t-t_0)} a_\omega(t_0) \right] \\ &+ \int_{-\infty}^{\infty} d\omega \gamma^2(\omega) \int_{t_0}^{t} dt' \left[ e^{i\omega(t-t')} X^+(t') \left[b,X^-\right] - \left[b,X^+\right] e^{-i\omega(t-t')} X^-(t') \right]. \end{aligned} \tag{5.16}$$

Under the RWA, only terms with $\omega \approx \omega_s$ contribute significantly, allowing us to replace $\gamma(\omega)$ by the constant value $\gamma(\omega_s)$. Setting

$$\gamma(\omega_s) = \sqrt{\eta/2\pi}, \tag{5.17}$$

(5.16) is reduced to

$$\dot{b} = -\frac{i}{\hbar}[b,H_{sys}] - \left[b,X^+\right] \left( \frac{\eta}{2} X^- + \sqrt{\eta} a_{in}(t) \right) + \left( \frac{\eta}{2} X^+ + \sqrt{\eta} a_{in}^\dagger(t) \right) \left[b,X^-\right], \tag{5.18}$$

where we have defined

$$a_{in}(t) = \frac{1}{\sqrt{2\pi}} \int_{-\infty}^{\infty} d\omega e^{-i\omega(t-t_0)} a_\omega(t_0). \tag{5.19}$$

The relation (5.18) is known as a *quantum Langevin equation* for the system operators $b$. Since $a_{in}(t)$ is the operator through which the bath affects the system, it can be thought of as an *input field*. Using (5.7) we obtain

$$\left[a_{in}(t),a_{in}^{\dagger}(t')\right] = \delta(t-t'). \tag{5.20}$$

To arrive at (5.18), we solved (5.14) in terms of an *initial condition* at $t_0 < t$. We can just as well, however, do it in terms of a *final condition* at $t_1 > t$. Defining

$$a_{out}(t) = \frac{1}{\sqrt{2\pi}} \int_{-\infty}^{\infty} d\omega e^{-i\omega(t-t_1)} b_{\omega}(t_1) \tag{5.21}$$

and proceeding with the same steps as above, the quantum Langevin equation can equivalently be written as

$$\begin{aligned} \dot{b} = -\frac{i}{\hbar}\left[b,H_{sys}\right] \quad &+ \quad \left[b,X^{+}\right]\left(\frac{\eta}{2}X^{-} - \sqrt{\eta}a_{out}(t)\right) \\ &- \quad \left(\frac{\eta}{2}X^{+} - \sqrt{\eta}a_{out}^{\dagger}(t)\right)\left[b,X^{-}\right]. \end{aligned} \tag{5.22}$$

The operator $a_{\mathrm{out}}(t)$ represents the state of the bath at future times, and can thus be though of as an *output field*. Now, combining (5.18) and (5.22), we obtain the result

$$a_{\mathrm{out}}(t) = a_{\mathrm{in}}(t) + \sqrt{\eta}X^{-}(t), \tag{5.23}$$

which is the input-output equation for our setup with a system locally coupled to a one-dimensional electromagnetic field. The input field $a_{\mathrm{in}}(t)$ can be specified independently of the system, whereas the output depends on the input and the system operator $X^{-}(t)$. For a multilevel system, (5.23) simply generalizes to

$$a_{\mathrm{out}}(t) = a_{\mathrm{in}}(t) + \sum_i \sqrt{\eta_i}X_i^{-}(t), \tag{5.24}$$

with

$$\eta_i = \frac{\pi\omega_i}{\hbar}\kappa^2(\omega_i). \tag{5.25}$$

As we saw in section (4.2), the quantum optical light-matter interaction is usually described by a pointlike electric dipole coupling. This corresponds to setting $\kappa(x) \propto \delta(x)$ in (5.5), which implies that $\kappa(\omega)$ is constant, reducing (5.8) to the electric dipole interaction (4.25). In some cases, the system

of interest is almost harmonic, like the transmon in section 2.7. For these systems, the effective coupling coefficients $\eta_i$ are approximately equal.

The derivations in this section can straightforwardly be modified to the case when the system is coupled to an infinite one-dimensional space, like an open transmission line. Here, the separate left- and right-moving fields are related to each other by input-output equations similar to (5.23) or (5.24). For a system coupled to several baths, we simply have a separate input-output equation for each one.

For the input-output equations to be useful, we need to know how the system state evolves and this is the role of the master equation, which can in principle be derived from the Langevin equation (5.18). We will, however, instead present a more traditional Bloch-Redfield derivation [135, 136], which gives a good insight into the physical significance of the various approximations used.

## 5.2 Master equations

In section 5.1, we derived equation (5.24), relating the input and output of a quantum system via the system operators. In order for this relation to be useful, however, we also need to determine how the input field influences the *state* of the system. This is the role of the master equation derived in this section. The input may consist of a coherent excitation, the *signal*, on top of a *noise* background. We first derive the master equation for the case with only the noise background present. The signal can later straightforwardly be added as a part of the free system Hamiltonian [133].

Let us start from a system-bath configuration with Hamiltonian $H = H_{\text{sys}} + H_B + H_{\text{int}}$, so that the total density operator $\rho(t)$ evolves unitarily according to the Liouville equation 5.3. Our aim is to find an equation for the *reduced* density operator of the system, obtained by tracing out the bath degrees of freedom,

$$\rho_{\text{sys}}(t) = \text{Tr}_B\left[\rho(t)\right]. \tag{5.26}$$

Starting in the Schrödinger picture, we first transform to the *interaction picture*, where an arbitrary operator is given by

$$\tilde{A}(t) = e^{\frac{i}{\hbar}(H_{\text{sys}}+H_{\text{B}})t} A e^{-\frac{i}{\hbar}(H_{\text{sys}}+H_{\text{B}})t}. \tag{5.27}$$

It is easy to show that, in the interaction picture, time-evolution is governed

solely by the interaction Hamiltonian,

$$\dot{\tilde{\rho}}(t) = -\frac{i}{\hbar}[\tilde{H}_{\rm int}(t), \tilde{\rho}(t)]. \tag{5.28}$$

We can integrate (5.28) to obtain

$$\tilde{\rho}(t) = \tilde{\rho}(0) - \frac{i}{\hbar}\int_0^t dt'[\tilde{H}_{\rm int}(t'), \tilde{\rho}(t')], \tag{5.29}$$

which substituted back into (5.28) yields

$$\dot{\tilde{\rho}}(t) = \frac{i}{\hbar}[\tilde{H}_{\rm int}(t), \tilde{\rho}(0)] - \frac{1}{\hbar^2}\int_0^t dt'[\tilde{H}_{\rm int}(t), [\tilde{H}_{\rm int}(t'), \tilde{\rho}(t')]]. \tag{5.30}$$

Now, by tracing (5.30) over the bath variables, we arrive at an equation for the reduced density operator in the interaction picture.

$$\dot{\tilde{\rho}}_{\rm sys}(t) = -\frac{1}{\hbar^2}\int_0^t dt' {\rm Tr}_B\left[[\tilde{H}_{\rm int}(t), [\tilde{H}_{\rm int}(t'), \tilde{\rho}(t')]]\right]. \tag{5.31}$$

To get rid of the first term in (5.30), we have assumed $\langle \tilde{H}_{\rm int}(t)\rangle_B = 0$, which can always be obtained by a redefinition of $H_{\rm sys}$ and $H_{\rm int}$. Now, in order to proceed from (5.31), we need to introduce some approximations.

First, we assume that the system and the bath are uncorrelated at $t = 0$, so that

$$\rho(0) = \tilde{\rho}(0) = \tilde{\rho}_{\rm sys}(0) \otimes \tilde{\rho}_B(0). \tag{5.32}$$

The following approximation relies on the assumption that the interaction is *weak* in the sense $H_{\rm int} \ll H_{\rm sys}, H_B$, and that the bath is large compared to the system. Under these conditions, the state of the bath is not significantly changed by the interaction, and we can take $\tilde{\rho}_B(t) = \tilde{\rho}_B(0) \equiv \rho_B$. Also, the density operator remains approximately a direct product for all times. These two assumptions can together be written as

$$\tilde{\rho}(t) \approx \tilde{\rho}_{\rm sys}(t) \otimes \rho_B, \tag{5.33}$$

which is known as the *Born approximation*. Inserting (5.33) into (5.31) yields

$$\dot{\tilde{\rho}}_{\rm sys}(t) = -\frac{1}{\hbar^2}\int_0^t dt' {\rm Tr}_B\left[[\tilde{H}_{\rm int}(t), [\tilde{H}_{\rm int}(t'), \tilde{\rho}_{\rm sys}(t') \otimes \rho_B]]\right]. \tag{5.34}$$

In this equation, $\dot{\tilde{\rho}}_{\rm sys}(t)$ depends on $\tilde{\rho}_{\rm sys}(t')$ at all earlier times $t' < t$. The goal of the next approximation is to eliminate this dependence and

turn (5.34) into a differential equation. This is achieved by making the replacement

$$\tilde{\rho}(t') \to \tilde{\rho}(t), \tag{5.35}$$

known as the *Markov approximation*.

To motivate the Markov approximation, we first assume that we can write the interaction Hamiltonian as a product of system and bath operators,

$$H_{\text{int}} = A_{\text{sys}} \otimes A_B. \tag{5.36}$$

This is no great restriction, and our Hamiltonian (5.5) for a system coupled to a Klein-Gordon field is of this form. Expanding the commutator in (5.34), each term will contain a correlation function of the form

$$f(t-t') \equiv \text{Tr}_B \left[ A_B(t) A_B(t') \rho_B \right]. \tag{5.37}$$

Now, suppose that the functions (5.37) are nonzero only for delay times $t - t'$ shorter than a characteristic bath correlation time $\tau_B$, and $\tilde{\rho}_{\text{sys}}(t)$ evolves on a characteristic timescale $\tau_{\text{sys}}$. If $\tau_B \ll \tau_{\text{sys}}$, $\tilde{\rho}_{\text{sys}}(t)$ stays approximately constant during the decay time of the correlation functions and we can safely make the Markov approximation. In practice, this is often the case since the timescale $\tau_{\text{sys}}$ is set by $H_{\text{int}}$, which is assumed to be small. For a quantum optical system coupled to a thermal bath, $\tau_B \ll \tau_{\text{sys}}$ is typically valid down to very low temperatures. Physically, the Markov approximation means that the bath has no memory when it comes to interactions with the system. A change in the bath induced by the system will have decayed before it can affect the system at a later time.

Applying the Markov approximation (5.35) to (5.34) and making a variable change results in

$$\dot{\tilde{\rho}}_{\text{sys}}(t) = -\frac{1}{\hbar^2} \int_0^\infty dt' \text{Tr}_B \left[ [\tilde{H}_{\text{int}}(t), [\tilde{H}_{\text{int}}(t-t'), \tilde{\rho}_{\text{sys}}(t) \otimes \rho_B]] \right], \tag{5.38}$$

where we also have extended the upper integration limit to $\infty$, which can be done due to the short bath correlation times. From the so-called *Born-Markov* master equation (5.38), we can derive a more specific quantum optical master equation by inserting the interaction Hamiltonian (5.8) and making further approximations.

In the interaction picture, the interaction Hamiltonian (5.8) becomes

$$\tilde{H}_{\text{int}}(t) = i \int_0^\infty d\omega \kappa(\omega) \sqrt{\frac{\hbar\omega}{2}} \left( a_\omega e^{-i\omega t} - a_\omega^\dagger e^{i\omega t} \right) \sum_i \left( X_i^+ e^{i\omega_i t} + X_i^- e^{-i\omega_i t} \right). \tag{5.39}$$

Using this expression, the next step is to expand the commutator in (5.38) and evaluate the integrals. This calculation involves correlation functions of the bath operators. Assuming a thermal bath state, these are

$$\langle a_\omega^\dagger a_{\omega'}\rangle = \mathrm{Tr}_B\left[a_\omega a_{\omega'}^\dagger \rho_\mathrm{B}\right] = \delta(\omega-\omega')n(\omega), \tag{5.40}$$

$$\langle a_\omega a_{\omega'}^\dagger\rangle = \mathrm{Tr}_B\left[a_\omega^\dagger a_{\omega'} \rho_\mathrm{B}\right] = \delta(\omega-\omega')\left(n(\omega)+1\right), \tag{5.41}$$

where $n(\omega)$ is the mean thermal photon number (4.47) at frequency $\omega$. The derivation also involves integrals of the type

$$\int_0^\infty e^{-i\omega t'} = \pi\delta(\omega) - i\mathcal{P}(\frac{1}{\omega}), \tag{5.42}$$

where $\mathcal{P}(1/\omega)$ gives rise to a principal value integral. In the end result, terms of this type leads to the Lamb shift mentioned in section (4.1.1) and the related Stark shift [137]. These are small renormalizations of the atomic energy levels and will be neglected in our derivation. The actual calculation is rather long and tedious and has been deferred to Appendix A. After evaluating the integrals, employing the RWA (see section 5.1), dropping the 'sys'-subscript and collecting the terms, we arrive at

$$\begin{aligned}\dot{\tilde{\rho}}(t) &= \frac{1}{2}\sum_i \eta_i\left(n(\omega_i)+1\right)\left(2X_i^-\tilde{\rho}(t)X_i^+ - \tilde{\rho}(t)X_i^+X_i^- - X_i^+X_i^-\tilde{\rho}(t)\right)\\ &+ \frac{1}{2}\sum_i \eta_i n(\omega_i)\left(2X_i^+\tilde{\rho}(t)X_i^- - \tilde{\rho}(t)X_i^-X_i^+ - X_i^-X_i^+\tilde{\rho}(t)\right),\end{aligned} \tag{5.43}$$

where $\eta_i$ is defined by (5.25). Transforming back to the Schrödinger picture and defining the *Lindblad superoperator*

$$\mathcal{D}\left[X\right]\rho = X\rho X^\dagger - \frac{1}{2}\left(X^\dagger X\rho - \rho X^\dagger X\right), \tag{5.44}$$

we can write (5.43) as

$$\dot{\rho}(t) = -\frac{i}{\hbar}[H_\mathrm{sys},\rho(t)] + \sum_i \eta_i\left[\left(n(\omega_i)+1\right)\mathcal{D}[X_i^-]\rho(t) + n(\omega_i)\mathcal{D}[X_i^+]\rho(t)\right]. \tag{5.45}$$

The equation (5.45) can be recognized as a *Lindblad master equation* [138]. The Lindblad formalism is a way to construct master equations to mathematically guarantee that the density operator remains physical. Here,

however, we arrived at a Lindblad equation using the more physical Bloch-Redfield derivation. The $\mathcal{D}[X^+]$-term describes thermal *excitations* of the system, while the $\mathcal{D}[X^-]$-term describes *relaxation*. Note that relaxation is present also in the case of negligible temperature. This is the phenomenon of spontaneous emission and is a consequence of the vacuum fluctuations.

Finally, let us generalize the master equation to accommodate the situation when a coherent input signal is present on top of the thermal noise. To include the coherent part, we make the replacement $a_\omega \to a_\omega + \alpha(\omega)$ in the Hamiltonian, with $\alpha(\omega) = \langle a_\omega \rangle$. Since the resulting extra terms contain no bath operators, they can be included in $H_{\text{sys}}$ and the derivation proceeds exactly as before. Suppose that the system is driven by a signal close to resonance with one of the transition frequencies $\omega_i$. In this case, after employing the RWA, the driving gives rise to the term

$$-\sqrt{\eta_i}\left[E_{\text{in}}(t)X_i^+ - E_{\text{in}}^*(t)X_i^-, \rho(t)\right] \tag{5.46}$$

at the right side of (5.45). Here, $E_{\text{in}}(t) \equiv \langle a_{\text{in}}(t) \rangle$ is the expectation value of the input field (5.19) and thus the Fourier transform of $\alpha(\omega)$ at the initial time $t_0$. Together with the input-output equation (5.24), the master equation specified by (5.45) and (5.46) can describe many situations of interest in quantum optics. In Papers I-IV, we use this type of equations when investigating a transmon coupled to coplanar waveguide with a coherent microwave driving signal.

Finally, it should be mentioned that the master equation is easily generalized to describe a system coupled to several baths. Often, in these cases, one of the baths represents a real transmission line containing the signal, while the remaining baths are fictional transmission lines modeling dissipation of the system into unknown channels.

## 5.3 Cascaded systems

In the previous two sections, we have developed a formalism for describing the output of a single quantum system, when the input has a coherent signal part and a thermal noise part. In this section, we extend the analysis to *cascaded quantum systems* [139, 140]. In these setups, the output of one system is used as input to a second system, without anything going in the reverse direction. Figure 5.1 shows a schematic sketch of two cascaded systems. To make sure that nothing is reflected back, a *circulator* is used. This is a three-port device which breaks time-reversal symmetry, so that

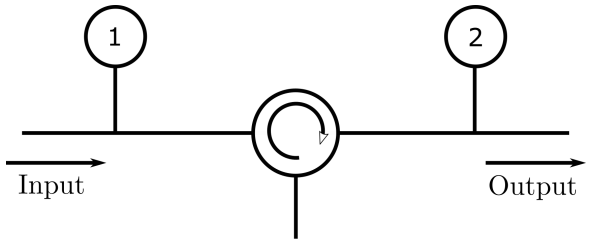


Figure 5.1: Schematic sketch of two cascaded systems. In the circulator, the signal always travels in the direction of the arrow, preventing any back-reflection from system 2 to system 1.

the signal always travels in the direction of the arrow (see figure 5.1). Unfortunately, the circulators in present day microwave technology are ferromagnetic off-chip devices that are both bulky and lossy. Realization of an efficient on-chip circulator would improve the performance of many proposed devices in circuit QED.

Apart from configurations with two or more real systems, the formalism of cascaded quantum systems can also be used to describe a single system being driven by a nonclassical signal. In this case, one makes use of an imaginary system producing the nonclassical output when driven by a coherent signal. This output is then fed into the input port of the real system under study. In Paper I, we use cascaded systems in a similar but slightly different way. To examine the effect of finite bandwidth in the measurement setup, we add an imaginary filter and cascade it with our system.

In [133], a master equation and input-output equations are derived for a setup with two cascaded systems. We will not repeat the derivations here, but simply state the results. We assume that both systems have a single transition around the same frequency $\omega_s$ and that the first system is driven with the coherent signal $E_{\rm in}(t)$. Subscripts 1 and 2 are used to denote the operators and couplings of the first and second system, respectively. Assuming no time delay for the signal to travel between the systems, the master equation for the total density operator becomes

$$\begin{aligned}\dot{\rho}(t) &= -\frac{i}{\hbar}[H_{\rm sys},\rho(t)] + \eta_1\mathcal{D}[X_1^-]\rho(t) + \eta_2\mathcal{D}[X_2^-]\rho(t) \\ &\quad -\sqrt{\eta_1\eta_2}\left([X_2^+, X_1^-\rho(t)] + [\rho(t)X_1^+, X_2^-]\right) \\ &\quad +\frac{n(\omega_s)}{2}\left[[\sqrt{\eta_1}X_1^- + \sqrt{\eta_2}X_2^-, \rho(t)], \sqrt{\eta_1}X_1^+ + \sqrt{\eta_2}X_2^+\right]\end{aligned} \tag{5.47}$$

$$
\begin{aligned}
&+\frac{n(\omega_s)}{2}\left[[\sqrt{\eta_1}X_1^+ + \sqrt{\eta_2}X_2^+, \rho(t)], \sqrt{\eta_1}X_1^- + \sqrt{\eta_2}X_2^-\right] \\
&-E_{\text{in}}(t)\left[\sqrt{\eta_1}X_1^+ + \sqrt{\eta_2}X_2^+, \rho(t)\right] \\
&-E_{\text{in}}^*(t)\left[\sqrt{\eta_1}X_1^- + \sqrt{\eta_2}X_2^-, \rho(t)\right].
\end{aligned}
$$

The asymmetry caused by the circulator is evident in the second row of (5.47). The output field from the second system is simply

$$a_{\text{out}}(t) = a_{\text{in}}(t) + \sqrt{\eta_1}X_1^-(t) + \sqrt{\eta_2}X_2^-(t), \tag{5.48}$$

where $a_{\text{in}}(t)$ in the input of the first system.

# Chapter 6

# Paper overview

In this chapter, we summarize the content in each of the six appended papers. Apart from stating the main ideas and results, we explain how the papers are related to the theories and methods introduced in Chapters 2-5. Moreover, my own contribution to each paper is briefly described.

## 6.1 Paper I - Generation of Nonclassical Microwave States Using an Artificial Atom in 1D Open Space

This paper is an experimental study of a transmon (see section 2.7) coupled to a one-dimensional open space in the form of a coplanar waveguide (see section 2.6). The transmon is driven with a stationary coherent microwave signal on resonance with the first transition, and the reflected and transmitted fields are measured. In the low-power limit, the incident coherent field is almost completely reflected due to destructive interference in the forward direction between the incident and scattered field. This extinction of the transmitted field has previously been shown with flux qubits [53, 141] and transmons [55].

In this paper, we investigate the quantum properties of the scattered field by measuring the second-order coherence function $g^{(2)}(\tau)$, defined in section 4.5.1. For low incident powers, it is shown that the transmitted field is superbunched, while the reflected field is antibunched. This means that the single-photon component of the incident coherent state (see section 4.4.2) is enhanced (suppressed) in the reflected (transmitted) field. In this

sense, the single artificial atom works as a *photon number filter*. In Paper IV, we investigate the possibility to exploit this effect for generations of single photons on demand.

For this paper, I contributed with the theoretical modeling of the experiment. The measured values of $g^{(2)}(0) > 0.55$ for the reflected field do not correspond to the well-known perfect antibunching $g^{(2)}(0) = 0$ expected from theory. Therefore, we had to take several experimental imperfections into account. The finite filter bandwidth in the processing of the signal is modeled by a transmission line resonator cascaded with the transmon, using the formalism described in section 5.3. The theoretical predictions show good agreement with the experimental data.

## 6.2 Paper II - Microwave quantum optics with an artificial atom in one-dimensional open space

This is a summary paper addressing the recent experimental advances in Paper I and [55]. Experimental results are presented in more detail. While both papers treat the same system, the experiments in [55] address three levels of the transmon. The Autler-Townes splitting (see section 6.3) of the energy levels is observed and applications for single-photon routing are discussed.

For this paper, apart from the part already included in Paper I, I contributed with assistance in some minor calculations on elastic and inelastic scattering.

## 6.3 Paper III - Scattering of coherent states on a single artificial atom

An atom coupled to a one-dimensional continuum of bosonic modes has been studied theoretically in [51, 52, 142–144] and experimental investigations in superconducting circuits include [53–55, 141, 145]. In this paper, we present a detailed theoretical analysis in the specific case of a transmon coupled to a transmission line. Part of the results is used in the theoretical modeling of the experiments in Papers I & II.

We start from a circuit model of a Cooper pair box coupled to a semi-infinite coplanar waveguide and make use of the circuit quantization procedure described in Chapter 2. The resulting equations of motion can in

a weak-coupling approximation be mapped onto quantum Langevin equations, from which we can derive input-output equations and a quantum optical master equation (see section 5.2). The results are readily generalized to a setup with an arbitrary number of transmission lines, including the important case of a single infinite line.

In the second part of the paper, the equations are applied to describe scattering of coherent input fields on a transmon in an open transmission line. Reflection and transmission coefficients are derived in the two-level and three-level approximations. In the two-level case, perfect reflection is approached for a resonant drive in the low-power limit. In the three-level case, we apply two coherent drives, one probe field at the first transition and one control field at the second transition. For large-amplitude control fields, we see almost full transmission for a weak probe field. This effect is due to a splitting of the atomic energy levels as a result of the driving field and is known as Autler-Townes splitting. By turning on and off the control field, we can switch between full reflection and full transmission for the probe field. This is the operating principle of the *single-photon router*, experimentally demonstrated in [55]. Finally, we analyze the second-order correlations of the scattered field in the two-level case. Including the effects of finite temperature and finite detection bandwidth, these results were used to model the experiment in Paper I.

For this paper, I contributed with the scattering calculations, as well as part of the derivations in the first section of the paper. I also wrote the corresponding parts of the manuscript.

## 6.4 Paper IV - Scattering of coherent pulses on a two-level system – single-photon generation

In Paper I, it was experimentally shown that scattering of a coherent field on a single two-level atom leads to a photon number redistribution in the scattered field. Specifically, the one-photon probability is enhanced in the reflected field compared to the incident coherent field. This raises the question of whether the setup can be exploited to generate single-photon states on demand. As mentioned in section 1.1, single-photon generation in circuit QED has been realized by using atoms coupled to cavities [63–66]. A drawback of these setups, however, is that the bandwidth of operation is limited by the cavity. A source based on a single atom without a cavity will not suffer from this problem and the frequency of the generated photons

can easily be controlled by tuning the resonance frequency of the atom.

The experiment in Paper I and the theoretical analysis in Paper III were done for stationary input fields. In order to achieve a true single-photon output field, however, the drive must have a finite duration. Thus, in this paper, we generalize the earlier calculations by analyzing the properties of the scattered field when the atom is driven by a coherent pulse. We determine the photon counting statistics of the reflected field and, specifically, the probability $P_1$ of generating exactly one photon. This is done by calculating higher-order correlation functions, i. e. generalizations of the non-normalized and non-stationary versions of $g^{(1)}(\tau)$ and $g^{(2)}(\tau)$ defined in section 4.5.1. The analysis does not only apply to circuit QED systems, but to any two-level system coupled to a continuum of photonic modes. A different example is surface plasmons in nanowires [146].

Our results show that, for pulses that are short compared to the relaxation time of the atom, $P_1 = 0.5$ can be achieved for appropriate input powers. This essentially corresponds to exciting the atom with a $\pi$-pulse and letting the photon leak out symmetrically in both directions. For an atom coupled to an infinite transmission line, this is the best we can do in terms of a single-photon source. In order to achieve higher one-photon probabilities, we can use a modified setup with two semi-infinite lines coupled to the atom; one weakly coupled and one strongly coupled. After exciting the atom with a $\pi$-pulse through the weakly coupled line, the photon leaks out in the strongly coupled line with high probability. A scheme of this type was later realized with a flux qubit [147].

For this paper, I performed all the calculations and wrote the manuscript.

## 6.5 Paper V - Twin paradox with macroscopic clocks in superconducting circuits

We saw in section 2.6.1 that a SQUID can be used to dynamically tune the boundary condition for the field in a coplanar waveguide, effectively simulating a moving mirror. This trick was used in [39] for simulation of a single oscillating mirror in order to demonstrate the dynamical Casimir effect. As suggested in [40], a similar setup with two SQUIDs may be used to simulate a moving cavity. By properly choosing the time-profile of the flux modulation in each SQUID, separate trajectories for the two mirrors can be realized in a way that corresponds to collective motion of the cavity. Moving cavities have recently been studied in the context of RQI to

investigate the effect of relativistic motion on entanglement and quantum information protocols [40, 75–79]. Possibly, superconducting circuits can serve as a platform to experimentally simulate these results.

In this paper, we propose an experiment where the moving cavity is used as a clock to observe time dilation (see section 3.1). The idea is to prepare the cavity field in a single-mode coherent state (see section 4.4.2). Since free time evolution of a coherent state simply corresponds to a phase rotation, the phase of the state can be used as a clock pointer. This requires that the mode frequency, and thus the length of the cavity, is kept constant. In other words, the motion of the cavity must be rigid (see section 3.2.2). During uniform acceleration, this is achieved by moving the mirrors along different hyperbolic trajectories. A more complicated trajectory can be realized by patching together segments of uniform acceleration and inertial motion.

To observe time dilation, we consider a twin paradox scenario (see section 3.1), with the trajectory shown in figure 6.1 A signal generator representing Alice's clock is used to prepare Rob's cavity clock in a coherent state. After flux-modulating the SQUIDs to simulate the trajectory, the field leaks out from the cavity and is mixed with the original signal. In this way, the relative phase shift between Alice's and Rob's clocks can be determined.

To compute the phase shift in Rob's cavity we employ field quantization in Rindler coordinates (see section 4.6) together with Bogoliubov transformation techniques (see section 4.7). Using experimentally realizable parameters, we find that the phase shift after a single trip is too small to be observable. Repeating the trajectory many times, however, we predict that accumulated phase shifts up to 130° can be achieved. Thus, the time dilation associated with the twin paradox scenario should be observable in our superconducting circuit system. At the moment, work is underway to perform the experiment at Chalmers.

The cavity clock described above can be seen as a fundamental model of a physical clock based on quantum field theory. This allows us to investigate deviations from an ideal clock that measures proper time along its path (see section 3.1). We find that, during the accelerated parts, the extension of the clock results in a slower tick rate. As the cavity becomes longer or the acceleration larger, the rate is slowed down. This effect should be observable for realistic circuit parameters. In addition, there is also a small deviation due to non-adiabatic effects. These depend on changes

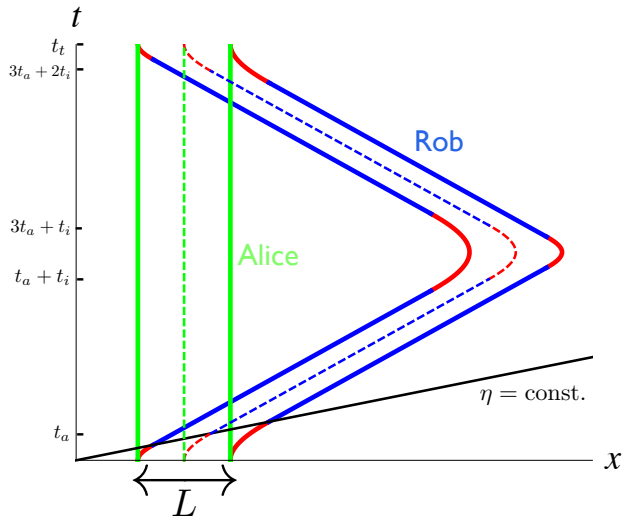


Figure 6.1: Cavity trajectories in the lab frame. Alice's cavity stays static, while Rob's cavity undergoes a round trip composed of segments of inertial motion (blue) and uniform acceleration (red). Figure taken from Paper V.

in acceleration and are encoded in the mode-mixing and particle creation coefficients in the Bogoliubov transformation (see section 4.7).

When applied to the vacuum, the particle creation coefficients account for the dynamical Casimir effect (see section 4.1.1). Since the photons created in this way are squeezed, the first moments of the field remain zero. When acting on a coherent state, however, the action of the $\beta$-coefficients can be understood as parametric pumping. In this case, a classical treatment gives the same result as the Bogoliubov transformation as far as the first moments of the field are concerned. Genuine quantum effects are seen in the second moments and this is investigated in Paper VI.

For this paper, I performed all the calculations. I also wrote most of the manuscript, with the exception of the introduction and the conclusions.

## 6.6 Paper VI - Motion and gravity effects in the precision of quantum clocks

In this paper, we extend the clock model of Paper V to theoretically investigate how motion affects the precision of the clock. We allow for arbitrary

single-mode Gaussian states (see section 4.4.4) in the cavity and use the covariance matrix formalism (see section 4.3) to implement the Bogoliubov transformations. Recall that both the Bogoliubov transformations and the tracing out of the higher modes preserves the Gaussian character of the state.

The precision is quantified by using techniques from *quantum parameter estimation* [148, 149] that have not been introduced in preceding chapters. Thus, a short introduction is in order here. Suppose that a quantity $\theta$, not itself an observable, parametrizes a family of states of a quantum system. Quantum parameter estimation addresses the problem of estimating the value of $\theta$ by performing quantum measurements on the system. If $M$ measurements are performed, the *Cramér-Rao inequality*,

$$\Delta\theta \geq \frac{1}{\sqrt{MH_\theta}}, \tag{6.1}$$

gives a lower bound on the variance $\Delta\theta$ in estimations of $\theta$. Here, $H_\theta$ is known as the *quantum Fisher information* (QFI).

In the case of our cavity clock, $\theta$ corresponds to the phase, parameterizing the family of single-mode Gaussian states. By computing the QFI for this case, we can thus determine the precision of the clock. It is investigated how the precision is affected by motion for a number of different initial states.

We find that the precision generally decreases as a result of non-uniform acceleration. This is mainly because photons are transferred from the clock mode due to mode-mixing. For a fixed number of photons, the optimal state for phase estimation is the squeezed vacuum. For this state, however, the degradation of the QFI due to motion is larger than for the coherent state. For states with both displacement and squeezing, the degradation depends on the squeezing angle. In the case of low-power initial states, particle creation effects start to become more important. For a coherent state with very few initial photons, the motion creates enough squeezed photons to enhance the QFI.

Finally, we also estimate the loss of precision in the proposed experiment in Paper V. When increasing the number of trajectories, we see a larger relative phase shift between Alice's and Rob's clocks. For longer travel times, however, more photons will have leaked from the cavity before the measurement takes place. This leads to a decrease of the QFI and, thus, there is a certain number of trajectories that optimizes the signal-to-noise ratio for phase estimation.

For this paper, I performed all the calculations. I also wrote the manuscript together with one of the co-authors.

# Chapter 7

# Summary and outlook

In this thesis, we have studied a number of systems which can be implemented in superconducting microwave circuits. The work has followed two main directions. The first is propagating microwaves interacting with artificial atoms and the second is relativistic motion of cavities, simulated by means of SQUIDs.

Superconducting qubits embedded in cavities have in the last decade grown into one of the main candidates for a future quantum computer. Propagating photons strongly interacting with artificial atoms is a more recent development with applications in quantum communication networks and possibly in all-optical quantum computing.

Inspired by ongoing experiments, we have studied a single transmon coupled to an open transmission line. Using the theoretical tools of circuit quantization, master equations and input-output equations, we derive equations to describe scattering of propagating coherent signals on the transmon. Through these calculations we are able to reproduce several results from recent experiments with propagating microwaves. Addressing only one transition of the transmon, we see full reflection in the low-power limit. Driving the second transition strongly, however, full transmission at the first transition is induced. We also see a photon number redistribution, with antibunching in the reflected field and superbunching in the transmitted field. These results agree with recent experiments and the effects all have possible applications in quantum networks.

As the next step, we investigate the possibilities of exploiting the photon number redistribution to generate single-photon states on demand. We find that a two-level system coupled to an open transmission line is

not a suitable single-photon source. With an asymmetric setup using two transmission lines, however, single-photon probabilities close to unity can be achieved. A similar setup was later realized in experiment [147] and, more recently, different non-cavity based single-photon sources have been proposed [150].

A reliable single-photon generator is only one of the various tools needed in order to realize on-chip quantum networks. Others include photon detectors, beam-splitters and sources of entangled states. More theoretical and experimental work with propagating microwaves coupled to artificial atoms remains to be done to complete the toolbox.

In the second part of the thesis, we have investigated a simple model of a fundamental clock based on quantum field theory. The clock consists of a rigid cavity where the fundamental mode is prepared in a Gaussian state, with a phase shift proportional to the elapsed time.

We propose an experiment where relativistic motion of the clock is simulated with SQUIDs in superconducting circuits, building on the idea used to demonstrate the dynamical Casimir effect [39]. We find that, for realistic circuit parameters, time dilation should be observable for the moving clock. The setup also lets us investigate how the rate of this macroscopic clock deviates from the ideal clock formula. Moreover, by using quantum estimation theory, we theoretically analyze how the accuracy of the clock is affected by motion. In general, we find that the precision is degraded due to non-uniform acceleration. Presently, theoretical work to model the experiment in more detail is underway, as well as preparations to perform the experiment.

In the future, the same experimental setup can possibly be used to simulate other results involving moving cavities, like the teleportation protocol in [40]. A much more challenging task would be to simulate a quantum superposition of two mirror trajectories. This can possibly be realized by using the setup in [151], where the field in a separate cavity is used to modulate the flux through the SQUID. By preparing the cavity field in a superposition of two coherent states, known as a cat state, a superposition of two flux signals tuning the SQUID can in principle be achieved. Moreover, as mentioned in section 1.2, there are also other proposals to simulate relativistic phenomena in superconducting circuits [80, 85, 118].

To sum up, we have used superconducting circuits both for quantum op-

tics setups aimed at quantum information technology and for simulation of relativistic physics. Despite the recent progress in both these areas, much is still to be explored before the full potential of superconducting circuits is realized.

# Appendix A

# Master equation derivation

In this Appendix, we fill in the details left out when going from (5.38) to (5.43) in the master equation derivation in section 5.2. Inserting the interaction Hamiltonian (5.39) into the Born-Markov master equation (5.38) yields

$$\begin{aligned}\dot{\tilde{\rho}}(t) &= \frac{1}{2\hbar}\int_0^\infty dt' \int_0^\infty d\omega \int_0^\infty d\omega' \kappa(\omega)\kappa(\omega')\sqrt{\omega\omega'} \\ &\quad \mathrm{Tr}_B\left[\left[\left(a_\omega(t) - a_\omega^\dagger(t)\right) X(t),\right.\right. \\ &\quad \left.\left.\left[\left(a_{\omega'}(t-t') - a_{\omega'}^\dagger(t-t')\right) X(t-t'), \tilde{\rho}(t)\otimes\rho_{\mathrm{B}}\right]\right]\right],\end{aligned} \tag{A.1}$$

with

$$X(t) = \sum_i \left(X_i^- e^{-i\omega_i t} + X_i^+ e^{i\omega t}\right) \tag{A.2}$$

and

$$a_\omega(t) = a_\omega e^{-i\omega t} \tag{A.3}$$

$$a_\omega^\dagger(t) = a_\omega^\dagger e^{i\omega t}. \tag{A.4}$$

Now, when evaluating the trace, the only nonzero bath correlation functions are (5.40)-(5.41). The double commutator in the the integrand becomes

$$\begin{aligned}&\langle a_\omega(t) a_{\omega'}^\dagger(t-t')\rangle \left(X(t-t')\tilde{\rho}(t)X(t) - X(t)X(t-t')\tilde{\rho}(t)\right) \\ &+\langle a_\omega^\dagger(t) a_{\omega'}(t-t')\rangle \left(X(t-t')\tilde{\rho}(t)X(t) - X(t)X(t-t')\tilde{\rho}(t)\right) \\ &+\langle a_{\omega'}(t-t') a_\omega^\dagger(t)\rangle \left(X(t)\tilde{\rho}(t)X(t-t') - \tilde{\rho}(t)X(t-t')X(t)\right)\end{aligned}$$

$$+\langle a^\dagger_{\omega'}(t-t')a_\omega(t)\rangle \left(X(t)\tilde{\rho}(t)X(t-t') - \tilde{\rho}(t)X(t-t')X(t)\right), \qquad \text{(A.5)}$$

where we have made use of the cyclic property of the trace. Using (5.40)-(5.41) and integrating over $\omega'$, we obtain

$$\begin{aligned}
& e^{-i\omega t'}\left(1+n(\omega)\right)\left[X(t-t')\tilde{\rho}(t)X(t) - X(t)X(t-t')\tilde{\rho}(t)\right] \\
+\;& e^{i\omega t'}n(\omega)\left[X(t-t')\tilde{\rho}(t)X(t) - X(t)X(t-t')\tilde{\rho}(t)\right] \\
+\;& e^{i\omega t'}\left(1+n(\omega)\right)\left[X(t)\tilde{\rho}(t)X(t-t') - \tilde{\rho}(t)X(t-t')X(t)\right] \\
+\;& e^{-i\omega t'}n(\omega)\left[X(t)\tilde{\rho}(t)X(t-t') - \tilde{\rho}(t)X(t-t')X(t)\right]. \qquad \text{(A.6)}
\end{aligned}$$

Next, we expand $X(t-t')$ according to (A.2) and integrate over $t'$. Using (5.42) and neglecting the second term, the result is

$$\begin{aligned}
& \pi\sum_i \left(1+n(\omega)\right)\left(X_i^- e^{-i\omega_i t}\delta(\omega-\omega_i) + X_i^+ e^{i\omega_i t}\delta(\omega+\omega_i)\right)\tilde{\rho}(t)X(t) \\
-\;& \pi\sum_i \left(1+n(\omega)\right)X(t)\left(X_i^- e^{-i\omega_i t}\delta(\omega-\omega_i) + X_i^+ e^{i\omega_i t}\delta(\omega+\omega_i)\right)\tilde{\rho}(t) \\
+\;& \pi\sum_i n(\omega)\left(X_i^- e^{-i\omega_i t}\delta(\omega+\omega_i) + X_i^+ e^{i\omega_i t}\delta(\omega-\omega_i)\right)\tilde{\rho}(t)X(t) \\
-\;& \pi\sum_i n(\omega)X(t)\left(X_i^- e^{-i\omega_i t}\delta(\omega+\omega_i) + X_i^+ e^{i\omega_i t}\delta(\omega-\omega_i)\right)\tilde{\rho}(t) \\
+\;& \pi\sum_i \left(1+n(\omega)\right)X(t)\tilde{\rho}(t)\left(X_i^- e^{-i\omega_i t}\delta(\omega+\omega_i) + X_i^+ e^{i\omega_i t}\delta(\omega-\omega_i)\right) \\
-\;& \pi\sum_i \left(1+n(\omega)\right)\tilde{\rho}(t)\left(X_i^- e^{-i\omega_i t}\delta(\omega+\omega_i) + X_i^+ e^{i\omega_i t}\delta(\omega-\omega_i)\right)X(t) \\
+\;& \pi\sum_i n(\omega)X(t)\tilde{\rho}(t)\left(X_i^- e^{-i\omega_i t}\delta(\omega-\omega_i) + X_i^+ e^{i\omega_i t}\delta(\omega+\omega_i)\right) \\
-\;& \pi\sum_i n(\omega)\tilde{\rho}(t)\left(X_i^- e^{-i\omega_i t}\delta(\omega-\omega_i) + X_i^+ e^{i\omega_i t}\delta(\omega+\omega_i)\right)X(t). \qquad \text{(A.7)}
\end{aligned}$$

Inserting (A.7) back into (A.1) and evaluating the $\omega$-integral, we arrive at

$$\begin{aligned}
\dot{\tilde{\rho}}(t) &= \frac{\pi}{2\hbar}\sum_i \kappa^2(\omega_i)\omega_i\left(n(\omega_i)+1\right)\left[X_i^-\tilde{\rho}(t)X(t) - X(t)X_i^-\tilde{\rho}(t)\right]e^{-i\omega_i t} \\
&+ \frac{\pi}{2\hbar}\sum_i \kappa^2(\omega_i)\omega_i n(\omega_i)\left[X_i^+\tilde{\rho}(t)X(t) - X(t)X_i^+\tilde{\rho}(t)\right]e^{i\omega_i t} \\
&+ \frac{\pi}{2\hbar}\sum_i \kappa^2(\omega_i)\omega_i\left(n(\omega_i)+1\right)\left[X(t)\tilde{\rho}(t)X_i^+ - \tilde{\rho}(t)X_i^+X(t)\right]e^{i\omega_i t}
\end{aligned}$$

$$+ \quad \frac{\pi}{2\hbar}\sum_i \kappa^2(\omega_i)\omega_i n(\omega)\left[X(t)\tilde{\rho}(t)X_i^- - \tilde{\rho}(t)X_i^- X(t)\right]e^{-i\omega_i t}. \quad \text{(A.8)}$$

When using the expansion $X(t) = \sum_i \left(X_j^- e^{-i\omega_j t} + X_j^+ e^{j\omega t}\right)$ and employing the RWA, only terms with $i = j$ survive as long as the transition frequencies are not too close to each other. This finally yields

$$\begin{aligned}\dot{\tilde{\rho}}(t) \;=\; & \frac{\pi}{2\hbar}\sum_i \kappa^2(\omega_i)\omega_i\left(n(\omega_i)+1\right) \qquad \text{(A.9)}\\ & \times\left(2X_i^-\tilde{\rho}(t)X_i^+ - \tilde{\rho}(t)X_i^+X_i^- - X_i^+X_i^-\tilde{\rho}(t)\right)\\ & +\frac{\pi}{2\hbar}\sum_i \kappa^2(\omega_i)\omega_i n(\omega_i)\left(2X_i^+\tilde{\rho}(t)X_i^- - \tilde{\rho}(t)X_i^-X_i^+ - X_i^-X_i^+\tilde{\rho}(t)\right),\end{aligned}$$

which, by the use of (5.25), is equivalent to (5.43).

# Bibliography


[1] S. Haroche, "Nobel Lecture: Controlling photons in a box and exploring the quantum to classical boundary", Rev. Mod. Phys. **85**, 1083 (2013).

[2] D. J. Wineland, "Nobel Lecture: Superposition, entanglement, and raising Schrödinger's cat", Rev. Mod. Phys. **85**, 1103 (2013).

[3] R. Miller, T. E. Northup, K. M. Birnbaum, A. Boca, A. D. Boozer, and H. J. Kimble, "Trapped atoms in cavity QED: coupling quantized light and matter", Journal of Physics B: Atomic, Molecular and Optical Physics **38**, S551 (2005).

[4] I. Buluta, S. Ashhab, and F. Nori, "Natural and artificial atoms for quantum computation", Reports on Progress in Physics **74**, 104401 (2011).

[5] A. Blais, R.-S. Huang, A. Wallraff, S. M. Girvin, and R. J. Schoelkopf, "Cavity quantum electrodynamics for superconducting electrical circuits: An architecture for quantum computation", Phys. Rev. A **69**, 062320 (2004).

[6] A. Wallraff, D. I. Schuster, A. Blais, L. Frunzio, R. S. Huang, J. Majer, S. Kumar, S. M. Girvin, and R. J. Schoelkopf, "Strong coupling of a single photon to a superconducting qubit using circuit quantum electrodynamics", Nature **431**, 162 (2004).

[7] R. J. Schoelkopf and S. M. Girvin, "Wiring up quantum systems", Nature **451**, 664 (2008).

[8] R. Feynman, "Simulating physics with computers", International Journal of Theoretical Physics **21**, 467 (1982).

[9] M. A. Nielsen and I. L. Chuang, *Quantum Computation and Quantum Information* (Cambridge University Press, 2000).

[10] L. K. Grover, "Quantum Mechanics Helps in Searching for a Needle in a Haystack", Phys. Rev. Lett. **79**, 325 (1997).

[11] A. W. Harrow, A. Hassidim, and S. Lloyd, "Quantum Algorithm for Linear Systems of Equations", Phys. Rev. Lett. **103**, 150502 (2009).

[12] P. Shor, "Algorithms for quantum computation: discrete logarithms and factoring", in Proceedings of the 35th annual symposium on foundations of computer science (1994), pp. 124–134.

[13] D. P. DiVincenzo, "The Physical Implementation of Quantum Computation", Fortschritte der Physik **48**, 771 (2000).

[14] J. I. Cirac and P. Zoller, "Quantum Computations with Cold Trapped Ions", Phys. Rev. Lett. **74**, 4091 (1995).

[15] J. I. Cirac and P. Zoller, "A scalable quantum computer with ions in an array of microtraps", Nature **404**, 579 (2000).

[16] D. Loss and D. P. DiVincenzo, "Quantum computation with quantum dots", Phys. Rev. A **57**, 120 (1998).

[17] R. Hanson, L. P. Kouwenhoven, J. R. Petta, S. Tarucha, and L. M. K. Vandersypen, "Spins in few-electron quantum dots", Rev. Mod. Phys. **79**, 1217 (2007).

[18] M. V. G. Dutt, L. Childress, L. Jiang, E. Togan, J. Maze, F. Jelezko, A. S. Zibrov, P. R. Hemmer, and M. D. Lukin, "Quantum Register Based on Individual Electronic and Nuclear Spin Qubits in Diamond", Science **316**, 1312 (2007).

[19] I. Bloch, "Quantum coherence and entanglement with ultracold atoms in optical lattices", Nature **453**, 1016 (2008).

[20] I. M. Georgescu, S. Ashhab, and F. Nori, "Quantum simulation", Rev. Mod. Phys. **86**, 153 (2014).

[21] N. Gisin and R. Thew, "Quantum communication", Nature Photonics **1**, 165 (2007).

[22] H. J. Kimble, "The quantum internet", Nature **453**, 1023 (2008).

[23] C. H. Bennett and G. Brassard, "Quantum cryptography: Public key distribution and coin tossing", in Proceedings of IEEE International Conference on Computers, Systems and Signal Processing (1984), pp. 175–179.

[24] H.-K. Lo, M. Curty, and K. Tamaki, "Secure quantum key distribution", Nature Photonics **8**, 595 (2014).

[25] A. Peres and D. R. Terno, "Quantum information and relativity theory", Rev. Mod. Phys. **76**, 93 (2004).

[26] P. M. Alsing and I. Fuentes, "Observer-dependent entanglement", Classical and Quantum Gravity **29**, 224001 (2012).

[27] W. Rindler, *Relativity: Special, General, and Cosmological* (Oxford University Press, 2001).

[28] S. Weinberg, *Gravitation and cosmology: principles and applications of the general theory of relativity* (Wiley, 1972).

[29] X.-S. Ma, T. Herbst, T. Scheidl, D. Wang, S. Kropatschek, W. Naylor, B. Wittmann, A. Mech, J. Kofler, E. Anisimova, V. Makarov, T. Jennewein, R. Ursin, and A. Zeilinger, "Quantum teleportation over 143 kilometres using active feed-forward", Nature **489**, 269 (2012).

[30] R. Ursin et al., "Space-quest, experiments with quantum entanglement in space", Europhysics News **40**, 26 (2009).

[31] Z. Merall, "Data teleportation: The quantum space race", Nature **492**, 22 (2012).

[32] M. Ahmadi, D. E. Bruschi, C. Sabín, G. Adesso, and I. Fuentes, "Relativistic Quantum Metrology: Exploiting relativity to improve quantum measurement technologies", Scientific Reports **4**, 4996 (2014).

[33] E. M. Kessler, P. Kómár, M. Bishof, L. Jiang, A. S. Sørensen, J. Ye, and M. D. Lukin, "Heisenberg-Limited Atom Clocks Based on Entangled Qubits", Phys. Rev. Lett. **112**, 190403 (2014).

[34] J. C. Hafele and R. E. Keating, "Around-the-World Atomic Clocks: Observed Relativistic Time Gains", Science **177**, 168 (1972).

[35] C. W. Chou, D. B. Hume, T. Rosenband, and D. J. Wineland, "Optical Clocks and Relativity", Science **329**, 1630 (2010).

[36] N. Ashby, "Relativity in the Global Positioning System", Living Reviews in Relativity **6** (2003).

[37] M. E. Peskin and D. V. Schroeder, *An Introduction to Quantum Field Theory* (Westview Press, 1995).

[38] N. D. Birrell and P. C. W. Davies, *Quantum Fields in Curved Space* (Cambridge University Press, 1984).

[39] C. M. Wilson, G. Johansson, A. Pourkabirian, M Simoen, J. R. Johansson, T. Duty, F. Nori, and P. Delsing, "Observation of the dynamical Casimir effect in a superconducting circuit", Nature **479**, 786 (1999).

[40] N. Friis, A. R. Lee, K. Truong, C. Sabín, E. Solano, G. Johansson, and I. Fuentes, "Relativistic Quantum Teleportation with Superconducting Circuits", Phys. Rev. Lett. **110**, 113602 (2013).

[41] B. D. Josephson, "Possible new effects in superconductive tunnelling", Phys. Lett. **1**, 251 (1962).

[42] D. M. Pozar, *Microwave Engineering*, 3rd ed. (John Wiley & Sons, Inc., 2005).

[43] Y. Nakamura, Y. A. Pashkin, and J. S. Tsai, "Coherent control of macroscopic quantum states in a single Cooper-pair box", Nature **398**, 786 (1999).

[44] C. H. van der Wal, A. C. J. ter Haar, F. K. Wilhelm, R. N. Schouten, C. J. P. M. Harmans, T. P. Orlando, S. Lloyd, and J. E. Mooij, "Quantum Superposition of Macroscopic Persistent-Current States", Science **290**, 773 (2000).

[45] I. Chiorescu, Y. Nakamura, C. J. P. M. Harmans, and J. E. Mooij, "Coherent Quantum Dynamics of a Superconducting Flux Qubit", Science **299**, 1869 (2003).

[46] J. M. Martinis, S. Nam, J. Aumentado, and C. Urbina, "Rabi Oscillations in a Large Josephson-Junction Qubit", Phys. Rev. Lett. **89**, 117901 (2002).

[47] J. Clarke and F. K. Wilhelm, "Superconducting quantum bits", Nature **453**, 1031 (2008).

[48] J. Koch, T. M. Yu, J. Gambetta, A. A. Houck, D. I. Schuster, J. Majer, A. Blais, M. H. Devoret, S. M. Girvin, and R. J. Schoelkopf, "Charge-insensitive qubit design derived from the Cooper pair box", Phys. Rev. A **76**, 042319 (2007).

[49] H. Paik, D. I. Schuster, L. S. Bishop, G. Kirchmair, G. Catelani, A. P. Sears, B. R. Johnson, M. J. Reagor, L. Frunzio, L. I. Glazman, S. M. Girvin, M. H. Devoret, and R. J. Schoelkopf, "Observation of High Coherence in Josephson Junction Qubits Measured in a Three-Dimensional Circuit QED Architecture", Phys. Rev. Lett. **107**, 240501 (2011).

[50] M. H. Devoret and R. J. Schoelkopf, "Superconducting Circuits for Quantum Information: An Outlook", Science **339**, 1169 (2013).

[51] J.-T. Shen and S. Fan, "Coherent Single Photon Transport in a One-Dimensional Waveguide Coupled with Superconducting Quantum Bits", Phys. Rev. Lett. **95**, 213001 (2005).

[52] H. Zheng, D. J. Gauthier, and H. U. Baranger, "Waveguide QED: Many-body bound-state effects in coherent and Fock-state scattering from a two-level system", Phys. Rev. A **82**, 063816 (2010).

[53] O. Astafiev, A. M. Zagoskin, A. A. Abdumalikov, Y. A. Pashkin, T. Yamamoto, K. Inomata, Y. Nakamura, and J. S. Tsai, "Resonance Fluorescence of a Single Artificial Atom", Science **327**, 840 (2010).

[54] A. A. Abdumalikov, O. V. Astafiev, Y. A. Pashkin, Y. Nakamura, and J. S. Tsai, "Dynamics of Coherent and Incoherent Emission from an Artificial Atom in a 1D Space", Phys. Rev. Lett. **107**, 043604 (2011).

[55] I.-C. Hoi, C. M. Wilson, G. Johansson, T. Palomaki, B. Peropadre, and P. Delsing, "Demonstration of a Single-Photon Router in the Microwave Regime", Phys. Rev. Lett. **107**, 073601 (2011).

[56] I.-C. Hoi, A. F. Kockum, T. Palomaki, T. M. Stace, B. Fan, L. Tornberg, S. R. Sathyamoorthy, G. Johansson, P. Delsing, and C. M. Wilson, "Giant Cross-Kerr Effect for Propagating Microwaves Induced by an Artificial Atom", Phys. Rev. Lett. **111**, 053601 (2013).

[57] I.-C. Hoi, "Quantum Optics with Propagating Microwaves in Superconducting Circuits", PhD thesis (Chalmers University of Technology, 2013).

[58] E. Knill, R. Laflamme, and G. J. Milburn, "A scheme for efficient quantum computation with linear optics", Nature **409**, 46 (2001).

[59] G. Romero, J. J. García-Ripoll, and E. Solano, "Microwave Photon Detector in Circuit QED", Phys. Rev. Lett. **102**, 173602 (2009).

[60] B. Peropadre, G. Romero, G. Johansson, C. M. Wilson, E. Solano, and J. J. García-Ripoll, "Approaching perfect microwave photodetection in circuit QED", Phys. Rev. A **84**, 063834 (2011).

[61] K. Koshino, K. Inomata, Z. Lin, Y. Nakamura, and T. Yamamoto, "Theory of microwave single-photon detection using an impedance-matched $\Lambda$ system", Phys. Rev. A **91**, 043805 (2015).

[62] S. R. Sathyamoorthy, L. Tornberg, A. F. Kockum, B. Q. Baragiola, J. Combes, C. M. Wilson, T. M. Stace, and G. Johansson, "Quantum Nondemolition Detection of a Propagating Microwave Photon", Phys. Rev. Lett. **112**, 093601 (2014).

[63] A. A. Houck, D. I. Schuster, J. M. Gambetta, J. A. Schreier, B. R. Johnson, J. M. Chow, L. Frunzio, J. Majer, M. H. Devoret, S. M. Girvin, and R. J. Schoelkopf, "Generating single microwave photons in a circuit", Nature **449**, 328 (2007).

[64] Y. Yin et al., "Catch and Release of Microwave Photon States", Phys. Rev. Lett. **110**, 107001 (2013).

[65] C. Lang, C. Eichler, L. Steffen, J. M. Fink, M. J. Woolley, A. Blais, and A. Wallraff, "Correlations, indistinguishability and entanglement in Hong-Ou-Mandel experiments at microwave frequencies", Nature Physics **9**, 345 (2013).

[66] M. Pechal, L. Huthmacher, C. Eichler, S. Zeytino ğlu, A. A. Abdumalikov, S. Berger, A. Wallraff, and S. Filipp, "Microwave-Controlled Generation of Shaped Single Photons in Circuit Quantum Electrodynamics", Phys. Rev. X **4**, 041010 (2014).

[67] Z.-L. Xiang, S. Ashhab, J. Q. You, and F. Nori, "Hybrid quantum circuits: Superconducting circuits interacting with other quantum systems", Rev. Mod. Phys. **85**, 623 (2013).

[68] M. Blencowe, "Quantum computing: Quantum RAM", Nature **468**, 44 (2010).

[69] J. D. Teufel, D. Li, M. S. Allman, K. Cicak, A. J. Sirois, J. D. Whittaker, and R. W. Simmonds, "Circuit cavity electromechanics in the strong-coupling regime", Nature **471**, 204 (2011).

[70] M. Aspelmeyer, T. J. Kippenberg, and F. Marquardt, "Cavity optomechanics", Rev. Mod. Phys. **86**, 1391 (2014).

[71] L. Diósi, "Models for universal reduction of macroscopic quantum fluctuations", Phys. Rev. A **40**, 1165 (1989).

[72] R. Penrose, "On Gravity's role in Quantum State Reduction", General Relativity and Gravitation **28**, 581 (1996).

[73] M. Blencowe, "Effective Field Theory Approach to Gravitationally Induced Decoherence", Phys. Rev. Lett. **111**, 021302 (2013).

[74] G. T. Moore, "Quantum Theory of the Electromagnetic Field in a Variable−Length One−Dimensional Cavity", Journal of Mathematical Physics **11**, 2679 (1970).

[75] T. G. Downes, I. Fuentes, and T. C. Ralph, "Entangling Moving Cavities in Noninertial Frames", Phys. Rev. Lett. **106**, 210502 (2011).

[76] N. Friis, D. E. Bruschi, J. Louko, and I. Fuentes, "Motion generates entanglement", Phys. Rev. D **85**, 081701 (2012).

[77] D. E. Bruschi, I. Fuentes, and J. Louko, "Voyage to Alpha Centauri: Entanglement degradation of cavity modes due to motion", Phys. Rev. D **85**, 061701 (2012).

[78] N. Friis, M. Huber, I. Fuentes, and D. E. Bruschi, "Quantum gates and multipartite entanglement resonances realized by nonuniform cavity motion", Phys. Rev. D **86**, 105003 (2012).

[79] D. E. Bruschi, A. Dragan, A. R. Lee, I. Fuentes, and J. Louko, "Relativistic Motion Generates Quantum Gates and Entanglement Resonances", Phys. Rev. Lett. **111**, 090504 (2013).

[80] S. Felicetti, C. Sabín, I. Fuentes, L. Lamata, G. Romero, and E. Solano, "Relativistic motion with superconducting qubits", Phys. Rev. B **92**, 064501 (2015).

[81] W. G. Unruh, "Notes on black-hole evaporation", Phys. Rev. D **14**, 870 (1976).

[82] M. O. Scully, V. V. Kocharovsky, A. Belyanin, E. Fry, and F. Capasso, "Enhancing Acceleration Radiation from Ground-State Atoms via Cavity Quantum Electrodynamics", Phys. Rev. Lett. **91**, 243004 (2003).

[83] S. W. Hawking, "Black hole explosions?", Nature **248**, 30 (1974).

[84] S. W. Hawking, "Particle creation by black holes", Communications in Mathematical Physics **43**, 199 (1975).

[85] P. D. Nation, M. P. Blencowe, A. J. Rimberg, and E. Buks, "Analogue Hawking Radiation in a dc-SQUID Array Transmission Line", Phys. Rev. Lett. **103**, 087004 (2009).

[86] M. Tinkham, *Introduction to Superconductivity*, 2nd ed. (Dover Publications, 2004).

[87] M. H. Devoret, "Quantum Fluctuations in Electrical Circuits", in Quantum Fluctuations, Les Houches, Session LXIII (1995), pp. 351–384.

[88] J. Bardeen, L. N. Cooper, and J. R. Schrieffer, "Theory of Superconductivity", Phys. Rev. **108**, 1175 (1957).

[89] L. N. Cooper, "Bound Electron Pairs in a Degenerate Fermi Gas", Phys. Rev. **104**, 1189 (1956).

[90] B. Yurke and J. S. Denker, "Quantum network theory", Phys. Rev. A **29**, 1419 (1984).

[91] J. J. Sakurai, *Modern Quantum Mechanics*, 2nd ed. (Addison-Wesley, 1994).

[92] U. Eckern, G. Schön, and V. Ambegaokar, "Quantum dynamics of a superconducting tunnel junction", Phys. Rev. B **30**, 6419 (1984).

[93] J. R. Johansson, G. Johansson, C. M. Wilson, and F. Nori, "Dynamical Casimir effect in superconducting microwave circuits", Phys. Rev. A **82**, 052509 (2010).

[94] J. R. Johansson, G. Johansson, C. M. Wilson, and F. Nori, "Dynamical Casimir Effect in a Superconducting Coplanar Waveguide", Phys. Rev. Lett. **103**, 147003 (2009).

[95] Y. Makhlin, G. Scöhn, and A. Shnirman, "Josephson-junction qubits with controlled couplings", Nature **398**, 305 (1999).

[96] A. Einstein, "Zur Elektrodynamik bewegter Körper", Annalen der Physik **322**, 891 (1905).

[97] H. Minkowski, "Die Grundgleichungen für die elektromagnetischen Vorgänge in bewegten Körpern", Mathematische Annalen **68**, 472 (1910).

[98] P. Langevin, Scientia **10**, 31 (1911).

[99] J. Bailey, K. Borer, F. Combley, H. Drumm, F. Krienen, F. Lange, E. Picasso, W. von Ruden, F. J. M. Farley, J. H. Field, W. Flegel, and P. M. Hattersley, "Measurements of relativistic time dilatation for positive and negative muons in a circular orbit", Nature **268**, 301 (1977).

[100] K. Lorek, J. Louko, and A. Dragan, "Ideal clocks – a convenient fiction", Classical and Quantum Gravity **32**, 175003 (2015).

[101] M. Born, "Die Theorie des starren Elektrons in der Kinematik des Relativitätsprinzips", Annalen der Physik **335**, 1 (1909).

[102] H. Nikolić, "Relativistic contraction of an accelerated rod", American Journal of Physics **67**, 1007 (1999).

[103] C. C. Gerry and P. L. Knight, *Introductory Quantum Optics* (Cambridge University Press, 2005).

[104] R. Loudon, *The Quantum Theory of Light* (Oxford University Press, 2000).

[105] G. Adesso, "Entanglement of Gaussian states", PhD thesis (University of Salerno, 2007).

[106] C. Weedbrook, S. Pirandola, R. García-Patrón, N. J. Cerf, T. C. Ralph, J. H. Shapiro, and S. Lloyd, "Gaussian quantum information", Rev. Mod. Phys. **84**, 621 (2012).

[107] W. E. Lamb and R. C. Retherford, "Fine Structure of the Hydrogen Atom by a Microwave Method", Phys. Rev. **72**, 241 (1947).

[108] H. A. Bethe, "The Electromagnetic Shift of Energy Levels", Phys. Rev. **72**, 339 (1947).

[109] V. Weisskopf and E. Wigner, "Berechnung der natürlichen Linienbreite auf Grund der Diracschen Lichttheorie", Zeitschrift für Physik **63**, 54 (1930).

[110] H. B. G. Casimir, "On the Attraction Between Two Perfectly Conducting Plates", Indag. Math. **10**, 261 (1948).

[111] M. J. Sparnaay, "Attractive forces between flat plates", Nature **180**, 334 (1957).

[112] S. K. Lamoreaux, "Demonstration of the Casimir Force in the 0.6 to 6$\mu$m Range", Phys. Rev. Lett. **78**, 5 (1997).

[113] U. Mohideen and A. Roy, "Precision Measurement of the Casimir Force from 0.1 to 0.9$\mu$m", Phys. Rev. Lett. **81**, 4549 (1998).

[114] S. A. Fulling and P. C. W. Davies, "Radiation from a Moving Mirror in Two Dimensional Space-Time: Conformal Anomaly", Proceedings of the Royal Society of London A: Mathematical, Physical and Engineering Sciences **348**, 393 (1976).

[115] A. Lambrecht, M.-T. Jaekel, and S. Reynaud, "Motion Induced Radiation from a Vibrating Cavity", Phys. Rev. Lett. **77**, 615 (1996).

[116] J. R. Johansson, G. Johansson, C. M. Wilson, P. Delsing, and F. Nori, "Nonclassical microwave radiation from the dynamical Casimir effect", Phys. Rev. A **87**, 043804 (2013).

[117] S. Felicetti, M. Sanz, L. Lamata, G. Romero, G. Johansson, P. Delsing, and E. Solano, "Dynamical Casimir Effect Entangles Artificial Atoms", Phys. Rev. Lett. **113**, 093602 (2014).

[118] P. D. Nation, J. R. Johansson, M. P. Blencowe, and F. Nori, "*Colloquium*: Stimulating uncertainty: Amplifying the quantum vacuum with superconducting circuits", Rev. Mod. Phys. **84**, 1 (2012).

[119] C. Riek, D. V. Seletskiy, A. S. Moskalenko, J. F. Schmidt, P. Krauspe, S. Eckart, S. Eggert, G. Burkard, and A. Leitenstorfer, "Direct sampling of electric-field vacuum fluctuations", Science **350**, 420 (2015).

[120] A. F. Kockum, P. Delsing, and G. Johansson, "Designing frequency-dependent relaxation rates and Lamb shifts for a giant artificial atom", Phys. Rev. A **90**, 013837 (2014).

[121] M. V. Gustafsson, T. Aref, A. F. Kockum, M. K. Ekström, G. Johansson, and P. Delsing, "Propagating phonons coupled to an artificial atom", Science **346**, 207 (2014).

[122] A. Ferraro, S. Olivares, and M. Paris, *Gaussian states in continuous variable quantum information* (Napoli Series on Physics and Astrophysics, 2005).

[123] R. J. Glauber, "Coherent and Incoherent States of the Radiation Field", Phys. Rev. **131**, 2766 (1963).

[124] M. Xiao, L.-A. Wu, and H. J. Kimble, "Precision measurement beyond the shot-noise limit", Phys. Rev. Lett. **59**, 278 (1987).

[125] H. Vahlbruch, S. Chelkowski, B. Hage, A. Franzen, K. Danzmann, and R. Schnabel, "Demonstration of a Squeezed-Light-Enhanced Power- and Signal-Recycled Michelson Interferometer", Phys. Rev. Lett. **95**, 211102 (2005).

[126] M. Aspachs, J. Calsamiglia, R. Muñoz Tapia, and E. Bagan, "Phase estimation for thermal Gaussian states", Phys. Rev. A **79**, 033834 (2009).

[127] R. J. Glauber, "The Quantum Theory of Optical Coherence", Phys. Rev. **130**, 2529 (1963).

[128] R. Hanbury Brown and R. Q. Twiss, "Correlation between Photons in two Coherent Beams of Light", Nature **177**, 27 (1956).

[129] M. P. da Silva, D. Bozyigit, A. Wallraff, and A. Blais, "Schemes for the observation of photon correlation functions in circuit QED with linear detectors", Phys. Rev. A **82**, 043804 (2010).

[130] L. C. B. Crispino, A. Higuchi, and G. E. A. Matsas, "The Unruh effect and its applications", Rev. Mod. Phys. **80**, 787 (2008).

[131] N. Friis and I. Fuentes, "Entanglement generation in relativistic quantum fields", Journal of Modern Optics **60**, 22 (2013).

[132] A. Caldeira and A. Leggett, "Quantum tunnelling in a dissipative system", Annals of Physics **149**, 374 (1983).

[133] C. Gardiner and P. Zoller, *Quantum Noise: A Handbook of Markovian and Non-Markovian Quantum Stochastic Methods with Applications to Quantum Optics*, 3rd ed. (Springer, 2004).

[134] C. W. Gardiner and M. J. Collett, "Input and output in damped quantum systems: Quantum stochastic differential equations and the master equation", Phys. Rev. A **31**, 3761 (1985).

[135] F. Bloch, "Generalized Theory of Relaxation", Phys. Rev. **105**, 1206 (1957).

[136] Redfield, A.G., "On the theory of relaxation processes", IBM Journal of Research and Development **1**, 19 (1957).

[137] J. Stark, "Beobachtungen über den Effekt des elektrischen Feldes auf Spektrallinien. I. Quereffekt", Annalen der Physik **348**, 965 (1914).

[138] G. Lindblad, "On the generators of quantum dynamical semigroups", Communications in Mathematical Physics **48**, 119 (1976).

[139] H. J. Carmichael, "Quantum trajectory theory for cascaded open systems", Phys. Rev. Lett. **70**, 2273 (1993).

[140] C. W. Gardiner, "Driving a quantum system with the output field from another driven quantum system", Phys. Rev. Lett. **70**, 2269 (1993).

[141] A. A. Abdumalikov, O. Astafiev, A. M. Zagoskin, Y. A. Pashkin, Y. Nakamura, and J. S. Tsai, "Electromagnetically Induced Transparency on a Single Artificial Atom", Phys. Rev. Lett. **104**, 193601 (2010).

[142] J. T. Shen and S. Fan, "Coherent photon transport from spontaneous emission in one-dimensional waveguides", Opt. Lett. **30**, 2001 (2005).

[143] H. Zheng, D. J. Gauthier, and H. U. Baranger, "Strongly correlated photons generated by coupling a three- or four-level system to a waveguide", Phys. Rev. A **85**, 043832 (2012).

[144] Ş. E. Kocabaş, E. Rephaeli, and S. Fan, "Resonance fluorescence in a waveguide geometry", Phys. Rev. A **85**, 023817 (2012).

[145] O. V. Astafiev, A. A. Abdumalikov, A. M. Zagoskin, Y. A. Pashkin, Y. Nakamura, and J. S. Tsai, "Ultimate On-Chip Quantum Amplifier", Phys. Rev. Lett. **104**, 183603 (2010).

[146] D. E. Chang, A. S. Sørensen, E. A. Demler, and M. D. Lukin, "A single-photon transistor using nanoscale surface plasmons", Nature Physics **3**, 807 (2007).

[147] Z. H. Peng, J. S. Tsai, and O. V. Astafiev, "Tunable on-demand single-photon source", arXiv:1505.05614 (2015).

[148] M. G. A. Paris, "Quantum Estimation for Quantum Technology", International Journal of Quantum Information **07**, 125 (2009).

[149] O. Pinel, P. Jian, N. Treps, C. Fabre, and D. Braun, "Quantum parameter estimation using general single-mode Gaussian states", Phys. Rev. A **88**, 040102 (2013).

[150] S. R. Sathyamoorthy, A. Bengtsson, P. Delsing, and G. Johansson, "Simple, robust and on-demand generation of single and correlated photons", arXiv:1511.03038 (2015).

[151] J. R. Johansson, G. Johansson, and F. Nori, "Optomechanical-like coupling between superconducting resonators", Phys. Rev. A **90**, 053833 (2014).